

# JGR Solid Earth



## RESEARCH ARTICLE

10.1029/2022JB025079

# Paleomagnetic Constraints From 925 Ma Mafic Dykes in North China and Brazil: Implications for the Paleogeography of Rodinia

Yuyang Hu<sup>1,2</sup> , Xixi Zhao<sup>3</sup> , Peng Peng<sup>4</sup> , Fengli Yang<sup>1,2</sup> , Manoel S. D'Agrella-Filho<sup>5</sup>, Weiwei Chen<sup>1,2</sup>, and Mingchen Xu<sup>1,2</sup>

<sup>1</sup>School of Ocean and Earth Science, Tongji University, Shanghai, China, <sup>2</sup>State Key Laboratory of Marine Geology, Tongji University, Shanghai, China, <sup>3</sup>Department of Ocean Science and Engineering, Southern University of Science and Technology, Shenzhen, China, <sup>4</sup>Institute of Geology and Geophysics, Chinese Academy of Sciences, Beijing, China, <sup>5</sup>Instituto de Astronomia, Geofísica e Ciências Atmosféricas, Universidade de São Paulo, São Paulo, Brazil

### Key Points:

- Characteristic remanence for the 925 Ma dykes in North China Craton and São Francisco Craton is interpreted as primary
- Both cratons were located at moderate–high paleolatitudes, southwest of Rodinia's core at 925 Ma, suggesting a paleogeographic connection
- The possible paleogeographic connection between the two cratons is supported by new paleomagnetic and geological evidence

### Supporting Information:

Supporting Information may be found in the online version of this article.

### Correspondence to:

X. Zhao and F. Yang,  
xzhao@tongji.edu.cn;  
yangfl@tongji.edu.cn

### Citation:

Hu, Y., Zhao, X., Peng, P., Yang, F., D'Agrella-Filho, M. S., Chen, W., & Xu, M. (2022). Paleomagnetic constraints from 925 Ma mafic dykes in North China and Brazil: Implications for the paleogeography of Rodinia. *Journal of Geophysical Research: Solid Earth*, 127, e2022JB025079. <https://doi.org/10.1029/2022JB025079>

Received 29 JUN 2022  
Accepted 14 SEP 2022

### Author Contributions:

**Data curation:** Yuyang Hu, Mingchen Xu  
**Formal analysis:** Weiwei Chen  
**Funding acquisition:** Xixi Zhao, Peng Peng, Fengli Yang  
**Investigation:** Yuyang Hu, Weiwei Chen  
**Software:** Mingchen Xu  
**Supervision:** Xixi Zhao, Fengli Yang  
**Validation:** Mingchen Xu  
**Visualization:** Yuyang Hu  
**Writing – original draft:** Yuyang Hu, Fengli Yang

© 2022. The Authors.

This is an open access article under the terms of the [Creative Commons Attribution License](https://creativecommons.org/licenses/by/4.0/), which permits use, distribution and reproduction in any medium, provided the original work is properly cited.

**Abstract** Coeval Neoproterozoic mafic dykes with a well-constrained isotopic age of 925 Ma are distributed in the North China Craton (NCC) of China and São Francisco Craton (SFC) of Brazil. Several recent studies favor the hypothesis that these two cratons were connected during 925 Ma and constituted building cratons for the supercontinent Rodinia. However, the paleo-positions of the two cratons in Rodinia have not yet been paleomagnetically resolved. This paper presents the paleomagnetic results of these dykes in both NCC and SFC. Detailed thermal and alternating-field demagnetization revealed that these dykes record stable components of magnetization with unblocking temperatures below the Curie temperature of magnetite. Rock magnetic results and scanning electron microscope analysis further confirm that the major magnetic minerals in dyke samples are pseudo-single domain titanomagnetites. The mean directions of the characteristic remanent magnetization (ChRM) of the dykes are distinct from those of rocks of different ages in the sampling localities, and are supported by positive baked contact tests, indicating primary remanent magnetization. The ChRM of the SFC dykes also exhibits dual polarity. Our results suggest that the NCC and SFC were in the moderate to high paleolatitudes of the Southern Hemisphere during approximately 925 Ma, suggesting a possible paleogeographic connection between the two cratons. A new paleogeographic reconstruction of both cratons during 925 Ma is proposed, which is supported by other geological evidence.

**Plain Language Summary** The formation and breakup of the supercontinent Rodinia have played crucial roles in the global tectonic evolution and paleoclimate changes during the Neoproterozoic which lasted from 1.0 billion to 541 million years ago. The exact configuration of the Rodinia remains debatable, including whether the North China Craton (NCC) and São Francisco Craton (SFC) were integral components of the Rodinia. In this paper, we present new results of an integrated investigation, including paleomagnetic and rock magnetic studies and scanning electron microscope analysis, on the well dated coeval 925 Ma mafic dykes in both NCC and SFC. The results of scanning electron microscope and magnetic measurements confirm the major magnetic minerals and the stability of characteristic remanence directions. The results imply that both NCC and SFC were located at moderate to high paleolatitudes of the Southern Hemisphere during approximately 925 Ma, suggesting the possibility of a paleogeographic connection between the two cratons in the Rodinia. The findings of this study help gain improved understanding of paleogeography of the early Earth.

## 1. Introduction

One of the most contentious topics in understanding the deep-time Earth history is supercontinent geodynamics, which has implications for determining the mechanisms of continent assembly and dispersal (e.g., Doucet et al., 2020; Nance & Murphy, 2013; Nance et al., 1988). It is generally believed that supercontinents, Nuna and Rodinia, were formed during Paleo-Neoproterozoic times, followed by the southern supercontinent Gondwana in the Neoproterozoic–Early Paleozoic, northern supercontinent Laurasia in Late Paleozoic, and the most recent supercontinent, Pangea at ~250 Ma. Over the past three decades, numerous efforts have been dedicated to the reconstruction of supercontinent's paleogeography in order to build a solid basis for supercontinent geodynamics (e.g., Evans et al., 2016; Nance & Murphy, 2013; Trindade et al., 2021).

Writing – review & editing: Fengli Yang, Manoel S. D'Agrella-Filho, Weiwei Chen

Rodinia supercontinent is believed to be unified by various Precambrian continental cratons during 1,300–900 Ma with the Grenville orogenic belt looping back around its core cratons. In recent years, the configuration of the Rodinia has attracted much attention and become the pivot point in supercontinent studies as sufficient geological data have been available. Rodinia also has a unique characteristic in that many of its building blocks are contingent with the well-studied Phanerozoic supercontinents Gondwana and Laurasia (e.g., Li & Zhong, 2009; Merdith et al., 2019; G. Zhao et al., 2018). Nevertheless, ever since the initial models describing the Rodinia were proposed in the 1990s (e.g., McMenamin & McMenamin, 1990), little consensus has been reached regarding its detailed configuration. In general, the larger core building cratons of the Rodinia, such as Laurentia, have been relatively well determined, forming the basic framework of the Rodinia (e.g., Merdith et al., 2017). The paleo-positions of smaller cratons of the Rodinia, however, are still controversial. In particular, the paleogeographic position of the Precambrian North China Craton (NCC) in the Rodinia is one of the most contentious issues, limiting the understanding of the tectonic history of the Rodinia.

The question of where the NCC should be placed in the Rodinia tended to be neglected in early reconstructions, such as in the “SWEAT” hypothesis (Moores, 1991), in which Rodinia was assembled on the basis of the geological correlation of the core cratons along the global-scale Grenville age orogenic belts. The NCC was identified as an integral component of the Rodinia for the first time in 1996 when the relatively detailed configurations of East Asian cratons became available (Li et al., 1996). In the reconstruction by Li et al. (1996), the present north margin of the NCC was placed adjacent to the southwestern margin of the Yenisei Ridge of Siberia from 1,800 to 600 Ma based on tectonostratigraphic correlations. This connection was partially supported by subsequent geologic records (Condie, 2002) and paleomagnetic results (S. Zhang et al., 2006). Subsequently, various models regarding the paleogeographic location of the NCC have been proposed based on the geological data, including (a) “NCC–São Francisco Craton (SFC)” connection (Cederberg et al., 2016; Chaves et al., 2019; Peng, Bleeker, et al., 2011), (b) “NCC–Baltica” connection (Fu et al., 2015), and (c) “NCC–Laurentia” connection (H. Zhao et al., 2020). The diversity of reconstructions emphasizes the need for additional Precambrian paleomagnetic poles for North China and other continents.

Mafic dyke swarms are considered as unique and useful geologic proxies for the paleogeographic reconstruction of supercontinents as they tend to be emplaced along continental margins or radiated out from a magmatic center from which plate breakup may take place. Coeval Neoproterozoic mafic dykes with a well-constrained isotopic age of 925 Ma are distributed in both NCC and SFC of Brazil. Peng, Bleeker, et al. (2011) suggested geographic proximities between the NCC and SFC, based mainly on the radiating pattern of the swarms and similar geochemistry of these mafic dykes aged at 925 Ma. Subsequent relevant research further discussed the possible geographic connection between NCC and SFC at that time and provided more evidence to support the model (Cederberg et al., 2016; Chaves et al., 2019; Su et al., 2021), such as the similar mid-ocean ridge basalt (MORB) compositions of the coeval dykes in the NCC and SFC and magmatic plumb systems indicating rift-to-drift transition.

Paleomagnetism plays a key role in quantitatively reconstructing the global paleogeography of continents during the Precambrian time. Recently reported paleomagnetic results have suggested that the connection between the NCC and SFC could even date back to the Mesoproterozoic (D'Agrella-Filho et al., 2020; Trindade et al., 2021).

Existing paleomagnetic databases, however, are far from complete in presenting a clear record of the paleogeographic connection between the NCC and SFC in the Precambrian. The quality and reliability of previously published paleomagnetic results from the 925 Ma mafic dykes in the NCC and SFC are widely variable, restricting the reliable constraining of the tectonic evolution of the two cratons (D'Agrella-Filho et al., 2004; Evans et al., 2016; Fu et al., 2015; S. Zhang et al., 2006).

This study aimed to better examine the age and distribution of dyke swarms that have been suggested to be related to the same radiating magma center (Peng, Bleeker, et al., 2011). To this end, a comparative paleomagnetic investigation was performed on the 925 Ma dykes in three widely distributed areas in central and northern parts of the NCC, and coeval dykes and sill from Salvador and Gentio do Ouro in northeast of the SFC (Figure 1). The new paleomagnetic data, coupled with geological correlations, further support for the hypothesis on the paleogeographic link between the NCC and SFC. A new paleogeographic reconstruction of the NCC and SFC in 925 Ma is proposed to advance our understanding of the tectonic evolution of the supercontinent Rodinia.

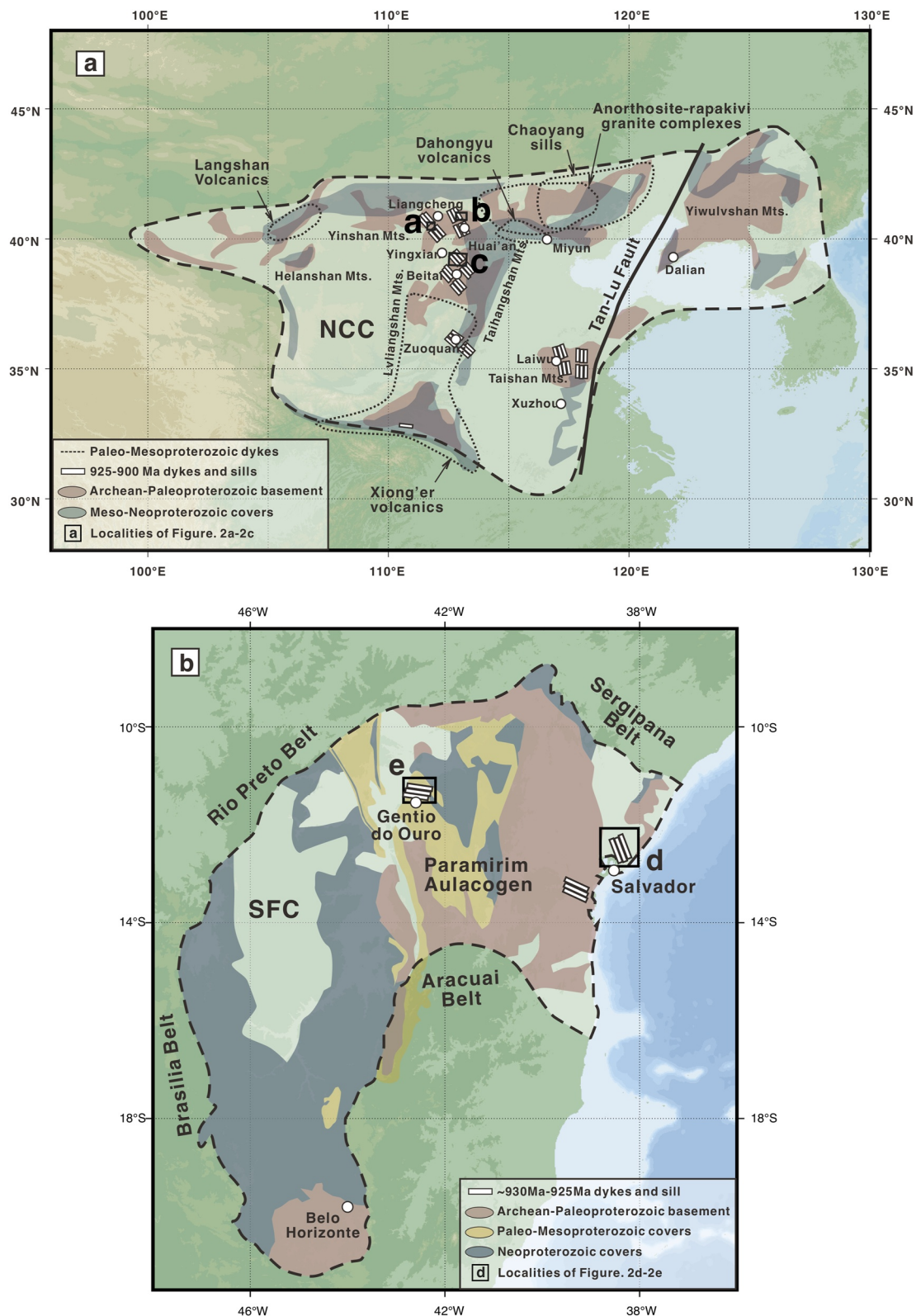


**Figure 1.** Regional maps showing (a) Distribution of Precambrian dykes, sills, and volcanics in the North China craton (NCC, 1,800–540 Ma), modified from Peng, Bleeker, et al. (2011). The dashed lines represent the boundary of the NCC. White circles: city names; Boxes and letters (a–c) sampling locations shown in Figures 2a–2c; (b) Distribution of ~930–925 Ma mafic dykes and sill in São Francisco Craton (SFC), modified from Moreira et al. (2020). The dashed lines represent the boundary of the SFC. White circles: city names; Boxes and letters (d–e) sampling locations shown in Figures 2d and 2e.

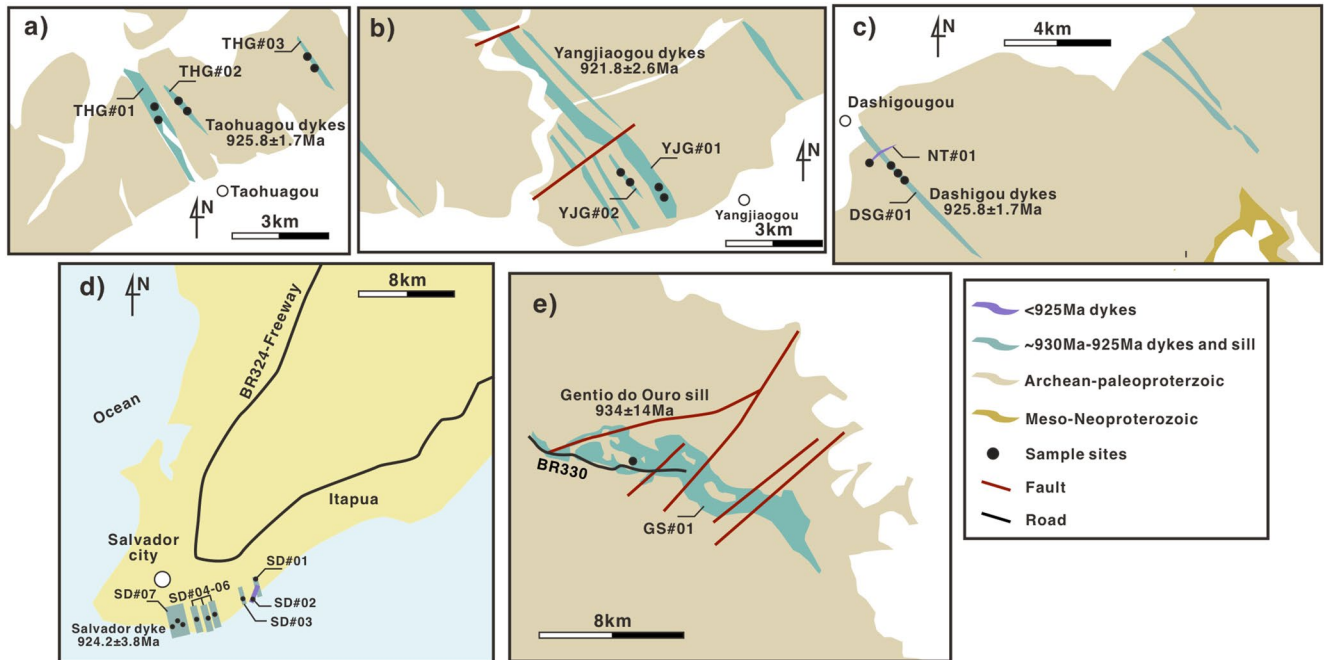


**Figure 2.** Enlarged maps showing the distribution of ~930–925 Ma mafic dykes and sill in the North China craton (NCC) and São Francisco Craton (SFC) (after D’Agrella-Filho et al., 2004; Loureiro et al., 2008; Peng, 2015a; Peng, Bleeker, et al., 2011). (a) dykes in the Taohuagou area of Inner Mongolia Autonomous Region, northern NCC, (b) dykes in the Yangjiaogou area of Hebei Province, central NCC, (c) dykes in the Dashigou area of Shanxi Province, central NCC, (d) dykes in Salvador of northeastern SFC, (e) mafic sill in Gento do Ouro of northern SFC. The location of Figures 2a–2e is shown in Figure 1.

## 2. Geological Setting

### 2.1. Precambrian Mafic Dykes in North China Craton

The NCC consists of several Archean blocks separated by three major Paleoproterozoic orogenic belts (e.g., G. Zhao & Cawood, 2012; S. Zhang et al., 2021). Various magmatic events ranging from late Paleoproterozoic to Neoproterozoic have been interpreted as response of the NCC to the evolution of supercontinents (e.g., Su et al., 2021; Zhai et al., 2015). As a consequence, multiple ages of Precambrian dykes and sills have been identified in the NCC. These dykes and sills, including the Taihang-Lvliang dyke swarm (1.78–1.77 Ga), Laiwu/Taishan dykes (1.68–1.63 Ga), Yanliao sill swarm (1.33 Ga), Tonghua-Bayan Obo dykes (1.23 Ga), Dashigou dyke swarm (925 Ma), and Sariwon sill swarm (900–890 Ma), intruded the crystalline basement and cover successions of the NCC (Peng, 2010, 2015b; Peng, Bleeker, et al., 2011, Peng, Zhai, et al., 2011; S. Zhang et al., 2021). These dykes of the NCC represent regionally widespread and short-lived magmatic events, with the features of a large igneous province (LIP) possibly triggered by a mantle plume (e.g., Bryan & Ernst, 2008).

The 925 Ma mafic dyke swarm has mainly been identified in the central part of the NCC. This swarm comprises the Dashigou dykes in central-northern Shanxi Province, Yangjiaogou dykes in northwestern Hebei Province, and Taohuagou dykes in Inner Mongolia Autonomous Region (Figures 1a and 2a–2c). The dykes in these regions typically trend about 305°–010°, dip vertically, and spread about 10–20 km with widths of 10–100 m. The mafic dykes comprise unmetamorphosed gabbro and diabase, with typical mineral assemblages of clinopyroxene (~30 vol.%) and plagioclase (~55 vol.%), and minor hornblende, K-feldspar and magnetite (Peng, 2015b). Precise measurements of U-Pb isotope dilution thermal ionization mass spectrometry (ID-TIMS) on baddeleyite grains obtained from three dyke groups yield  $^{207}\text{Pb}/^{206}\text{Pb}$  average ages of  $924.0 \pm 3.7$  Ma (Dashigou dykes),  $921.8 \pm 2.6$  Ma (Yangjiaogou dykes) and  $925.8 \pm 1.7$  Ma (Taohuagou dykes) (Peng, Bleeker, et al., 2011). The 925 Ma dykes exhibit an overall radiating geometry, with a focal point at the southeastern NCC and an overall fan angle of ~60° (Su et al., 2021). The geochemical characteristics of these dykes correspond to OIB (Oceanic Island Basalt) and MORB. These characteristics indicate that the giant 925 Ma mafic dykes were originated from a mantle source in the asthenosphere centered along the present southern margin of the eastern NCC, representing a LIP event (Peng, Bleeker, et al., 2011; Su et al., 2021).

## 2.2. Precambrian Mafic Dykes in São Francisco Craton

The São Francisco Craton of Northeastern Brazil, considered as an extension of the Congo Craton in the Africa continent, is composed of several Archean to Paleoproterozoic blocks amalgamated during Paleoproterozoic orogenesis (2.2–1.8 Ga) (Figure 1b; e.g., Padilha et al., 2019). The craton is extensively overlain by Proterozoic and Phanerozoic sedimentary sequences and is one of the most ancient shield areas across the globe. However, only two main Archean-Paleoproterozoic portions of the basement are exposed in the southern and northeastern cratonic margin (e.g., Teixeira et al., 2017). The final amalgamation of the Congo-São Francisco Craton (Trindade et al., 2021) is mainly recorded in two Paleoproterozoic mobile belts: (a) the Itabuna-Salvador-Curaçá belt in the northeastern SFC, whose rocks reached high-degree metamorphism (Barbosa et al., 2008), and (b) the Mineiro belt in the southern SFC, which consists of granitoids and a volcano-sedimentary succession metamorphosed at greenschist to amphibolite facies (Alkmim & Marshak, 1998). Following the amalgamation, several mafic dyke swarms of similar compositions and ages were emplaced on the coastline of the northeastern SFC during the early Neoproterozoic, in response to the post-assembly extension (Chaves et al., 2019).

The Bahia radiating dyke swarm, mainly comprising the Salvador and Ilhéus-Oliveira dykes, is located in the northeastern part of the SFC (Figure 1b; Evans et al., 2016). The NNW trending Salvador dykes crosscut granulites of polycyclic terrains dominantly formed/reworked during the Paleoproterozoic (Chaves et al., 2019; Evans et al., 2016). The dykes have a general width of less than 5 m and a maximum width of 50 m. The dykes are mainly composed of unmetamorphosed diabase, consisting of plagioclase, clinopyroxene, some olivine, and ilmenite distributed in a primary subophitic igneous texture (Correa-Gomes & Oliveira, 2000). The E-W trending Ilhéus-Oliveira dykes are distributed along the Atlantic coastline south of the Salvador dyke. Numerous precise chronology data of the Bahia radiating dyke swarm have been reported in recent years. Newly reported U-Pb baddeleyite ages are  $921.5 \pm 4.3$  and  $924.2 \pm 3.8$  Ma for diabase dykes from Salvador and  $926.1 \pm 4.6$  and  $918.2 \pm 6.7$  Ma for dykes from Ilhéus-Oliveira, ~450 km south of Salvador (Evans et al., 2016). The two dyke sets exhibit comparable petrologic and geochemical features, suggesting that they are coeval (Bellieni et al., 1998). In addition, coeval mafic sill has been identified from Gentio do Ouro, ~480 km northwest of Salvador and dated at  $934 \pm 14$  Ma (Figures 2d and 2e; Loureiro et al., 2008). The Bahia dyke swarm has also been proposed to be characterized by a single intraplate magmatic event, with short duration of the emplacement, similar to that of a LIP event (Ernst & Buchan, 1997). The Bahia radiating dyke swarm mainly comprises unmetamorphosed tholeiitic and andesitic basalts (Chaves et al., 2019), which are suitable materials for paleomagnetic study.

## 3. Paleomagnetic Sampling and Measurements

### 3.1. Paleomagnetic Sampling

We collected standard oriented cylindrical cores with a portable, gasoline-powered rock drill from dykes in the Dashigou area of Shanxi Province, Taohuagou area of Inner Mongolia Autonomous Region, and Yangjiaogou area of Hebei Province in the NCC, and the Salvador dykes and Gentio do Ouro sill of Bahia State in the SFC (Figures 2a–2d). A total of 189 paleomagnetic samples were collected from six 925 Ma dykes in the NCC, including three sites from a dyke in Dashigou, six sites from three dykes in Taohuagou and four sites from two dykes in Yangjiaogou. In addition, two sites from a fresh young dyke (NT#01), which is about 350 m west of the Dashigou dyke DSG#01 and is dated at ~30 Ma (Peng, 2015a; Tang et al., 2012), were also collected to check the stability of the 925 Ma Dashigou dyke (Figures 2a–2c). Similarly, seven dykes and one sill with a total of 141 samples were collected from the SFC, including eight sites from six 925 Ma Salvador dykes, one site from a younger undated dyke (SD#02) and one site from the  $934 \pm 14$  Ma Gentio do Ouro sill (Figures 2d and 2e). Field samples were oriented using both sun and magnetic compasses with a clinometer, and trimmed into 2.2 cm long cylinders for subsequent paleomagnetic analysis. Selected core chips were used for rock magnetic measurements.

The dykes at both cratons lack directly overlying cover strata, preventing the possibility of performing fold and tilt tests. In an attempt to constrain the age of remanence acquisition and detect possible overprints, we also collected paleomagnetic samples for baked contact tests in both cratons. In the NCC, 13 samples were collected from a ~1.95 Ga porphyritic garnet granite (Figure S1a in Supporting Information S1; Peng, Bleeker, et al., 2011; Wang et al., 2017) that is in contact with dyke THG#01. In the SFC, six samples were collected from Paleoproterozoic granulites (Figure S1b in Supporting Information S1; D'Agrella-Filho et al., 2004), which was intruded by the 925 Ma dyke (SD#06).

### 3.2. Paleomagnetic and Rock Magnetic Measurements and Analytical Methods

All the magnetic measurements were carried out in a magnetically shielded room. Samples were subjected to progressive thermal and alternating field (AF) demagnetization and measurements were taken at each stage of treatment at the Paleomagnetism Labs of the State Key Laboratory of Marine Geology, Tongji University, China and of the University of California at Santa Cruz, USA.

Based on the AF demagnetization results yielded from pilot samples, the stepwise thermal demagnetization was adopted as the primary method for most samples with temperature steps ranging from 50°C to 100°C at low temperature to 5°C–20°C above 400°C in the TD48SC thermal demagnetizer. Remanent magnetization was determined using both the JR-6A spinner magnetometer and the 2G-Enterprise SQUID magnetometer with precision ranges of  $2.0 \times 10^{-6}$ – $12.5 \times 10^3$  A/m and  $1.0 \times 10^{-12}$ – $2.0 \times 10^{-3}$  Am<sup>2</sup>, respectively. Magnetization directions were determined through principal component analysis (PCA) (Kirschvink, 1980) and the magnetic components for each specimen were analyzed using orthogonal plots (Zijderveld, 1967). The site mean directions of all demagnetized data were derived by assigning a unit weight to each mean sample direction and calculated through Fisher statistics (Fisher, 1953).

The anisotropy of magnetic susceptibility (AMS) was measured to examine the preferred orientations of magnetic mineral fabrics and infer the nature of magma transport (vertical or lateral). The AMS measurements were conducted using the MFK1 Kappabridge susceptometer and the AMS data were statistically analyzed using ANISOFT v.5.1, through which site-average AMS parameters were calculated (Flinn, 1965). The rock magnetic measurements were performed in the paleomagnetic laboratory of the University of California Santa Cruz, within which thermomagnetic analysis of magnetic susceptibility (*K-T* curves) was conducted on a CS-4 apparatus coupled to a Kappabridge instrument and hysteresis experiments were performed using a MicroMag Vibrating Sample Magnetometer.

### 3.3. Scanning Electron Microscope Measurement

Scanning electron microscope (SEM) analyses were performed on six representative dyke samples from both the NCC and SFC to identify magnetic minerals. Each sample was loaded onto acrylic disks, impregnated, and subjected to carbon metalization, and finally analyzed using SEM. The analysis was conducted in the SEM Lab of the State Key Laboratory of Marine Geology, Tongji University, using the TESCAN MIRA3 FEG-SEM with the Oxford Instruments Ultim Max 40 EDS (energy-dispersive X-ray spectroscopy) for semi-quantitative analysis.

## 4. Results

### 4.1. AMS Results

For the AMS measurements, we selected a total of 40 representative samples of the 925 Ma dykes of the NCC and 55 samples of the coeval dykes in SFC. The mean magnetic susceptibility values of NCC samples were in the range of  $1.016 \times 10^{-3}$ – $26.35 \times 10^{-3}$  SI units and the bulk mean susceptibility ( $K_m$ ) was  $12.53 \times 10^{-3}$  SI units (Figure S2a in Supporting Information S1). The degree of anisotropy ( $P_j$ ) and shape parameter ( $T$ ) ranged from 1.005 to 1.062 and from  $-0.948$  to 0.930, respectively, with no correlation between the two parameters (Figure S2b in Supporting Information S1). For the 55 samples from the SFC, the mean magnetic susceptibility ranges from  $12.61 \times 10^{-3}$  to  $111.4 \times 10^{-3}$  SI units and the bulk mean susceptibility ( $K_m$ ) was  $45.79 \times 10^{-3}$  SI units (Figure S2c in Supporting Information S1). The degree of anisotropy ( $P_j$ ) and shape parameter ( $T$ ) ranged from 1.021 to 1.092 and from  $-0.920$  to 0.678, respectively, also with no correlation between them (Figure S2d in Supporting Information S1). Thus, the samples from both cratons showed similar values of the AMS parameters. In light of the low degree of anisotropy, we consider it very unlikely that the remanent magnetic directions of the 925 Ma dykes from both cratons could have been significantly affected by deformation. Moreover, the values of parameter  $P_j$  are less than 1.2, which has been suggested to indicate a primary magmatic flow fabric (Hrouda, 1982).

Following Knight and Walker (1988), we refer a normal magnetic fabric with the magnetic foliation ( $K_{max}$ – $K_{int}$  plane) approximately parallel to the trend of the dykes and  $K_{min}$  perpendicular to the dyke wall plane. Samples from dyke DSG#01 were characterized by a normal magnetic fabric (Figure S3a in Supporting Information S1), whereas samples from the Taohuagou and Yangjiaogou dykes were characterized by  $K_{max}$  approximately

perpendicular to the dyke wall plane and the  $K_{\text{int}}-K_{\text{min}}$  plane parallel to the trend of the dykes (Figures S3b and S3c in Supporting Information S1). The orientations of the  $K_{\text{max}}$  and  $K_{\text{int}}$  axes of the normal magnetic fabrics of the NCC samples indicate lateral magma flow with an approximate NW-SE trend according to the low inclination and the plane defined by the  $K_{\text{max}}$  and  $K_{\text{int}}$  axes. In the SFC, only one site from dyke SD#03 could be characterized by a normal magnetic fabric (Figure S4b in Supporting Information S1). In the remaining sites,  $K_{\text{int}}$  is approximately perpendicular to the dyke wall plane and the  $K_{\text{max}}-K_{\text{min}}$  plane is parallel to the trend of the dykes (Figure S4 in Supporting Information S1). The low inclination and the plane defined by the  $K_{\text{max}}$  and  $K_{\text{int}}$  axes suggest lateral magma flow with an approximate NW-SE trend, consistent with the results of the NCC.

#### 4.2. Thermomagnetic Results and Hysteresis Properties

Thermomagnetic curves of the 925 Ma dyke samples from both the NCC and SFC displayed two types. Type I curves showed a slight increase in magnetic moment with heating at 150°C–180°C and nonreversible cooling curves (Figure 3a). Cooling curves showed slightly higher magnetization than the heating curves, which may reflect the formation of additional magnetite. Type II curves showed nearly reversible heating and cooling curves with Curie temperatures ranging from 560°C to 585°C and exhibited a Hopkinson peak before dropping rapidly at 580°C (Figure 3b), indicative of the presence of titanomagnetite.

The hysteresis curves for representative samples from both cratons were similar, yielding relatively low bulk coercive field ( $B_c$ ) and coercivity of remanence ( $B_{cr}$ ) (<100 mT) with the ratio of saturation remanence ( $M_r$ ) and saturation magnetization ( $M_s$ ) in the range of 0.15–0.3, corresponding to the region for pseudo-single domain behavior (Day et al., 1977). The hysteresis behavior of the dykes suggests that samples from both the NCC and SFC mainly contain titanomagnetite as the magnetic mineral (Figures 3c and 3d).

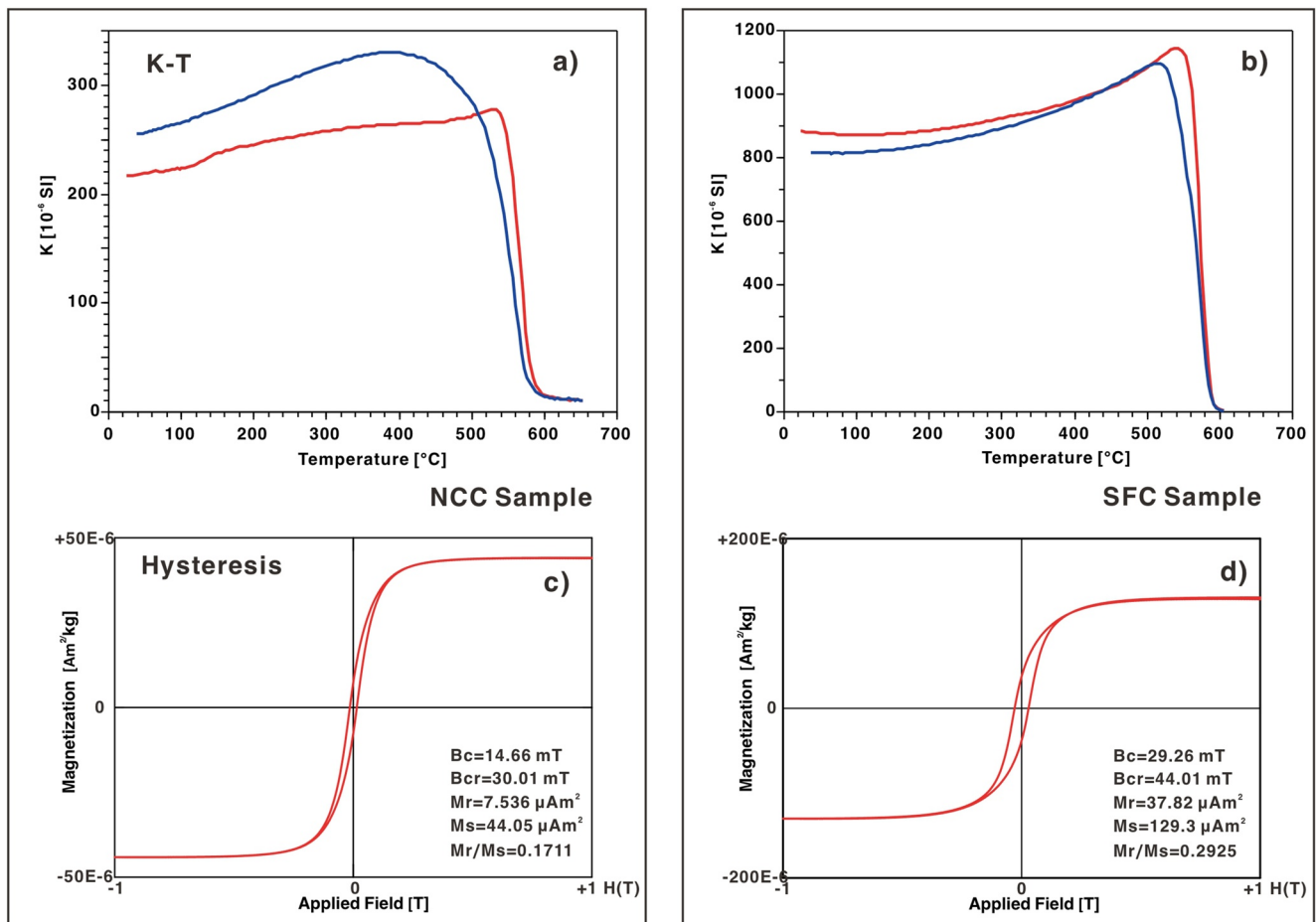


**Figure 3.** Thermomagnetic analysis plots (susceptibility vs. temperature) and hysteresis loop for representative dyke samples of (a), (c) North China craton (NCC), and (b), (d) São Francisco Craton (SFC). The red and blue curves represent heating and cooling, respectively.

### 4.3. Results From Scanning Electron Microscope (SEM) and Energy Dispersive X-ray Spectroscopy (EDS)

The combined SEM-EDS analysis was performed on the representative samples of the 925 Ma dykes from both NCC and SFC to identify the magnetic minerals involved. According to the SEM images, titanomagnetite is the major magnetic mineral for samples from both cratons, characterized by the higher luminance in back-scattered electron detector (BSE) images (Figure 4). The elements in metal minerals are mainly oxygen, iron and titanium, and do not contain sulfur. The major axes of single titanomagnetite are mainly less than 50  $\mu\text{m}$  (Figure 4). The SEM-EDS results of the NCC samples reveal that low-titanium titanomagnetite is the main magnetic mineral in the 925 Ma dykes, consistent with the demagnetization curves of the dyke samples showing unblocking temperatures ranging from 550°C to 580°C (Figures 5a–5e). The SFC samples exhibited additional finer titanomagnetite grains with major axes ranged in 2–5  $\mu\text{m}$  (Figure 4b), which have been suggested to be capable of carrying primary remanent magnetization (D’Agrella-Filho et al., 1990; Raposo & Berquó, 2008). In BSE images, magnetic minerals are characterized by subeuhedral and even euhedral crystals with relatively complete crystal morphology, indicating that they are likely primary minerals and have not been strongly affected by chemical alteration and weathering. Moreover, the shapes of iron oxides are irregular, and they do not grow in the boundaries and crystal cracks of other minerals. The SEM-EDS results in combination with rock magnetic data suggest that magnetization is mainly carried by low-titanium titanomagnetite in PSD grains.

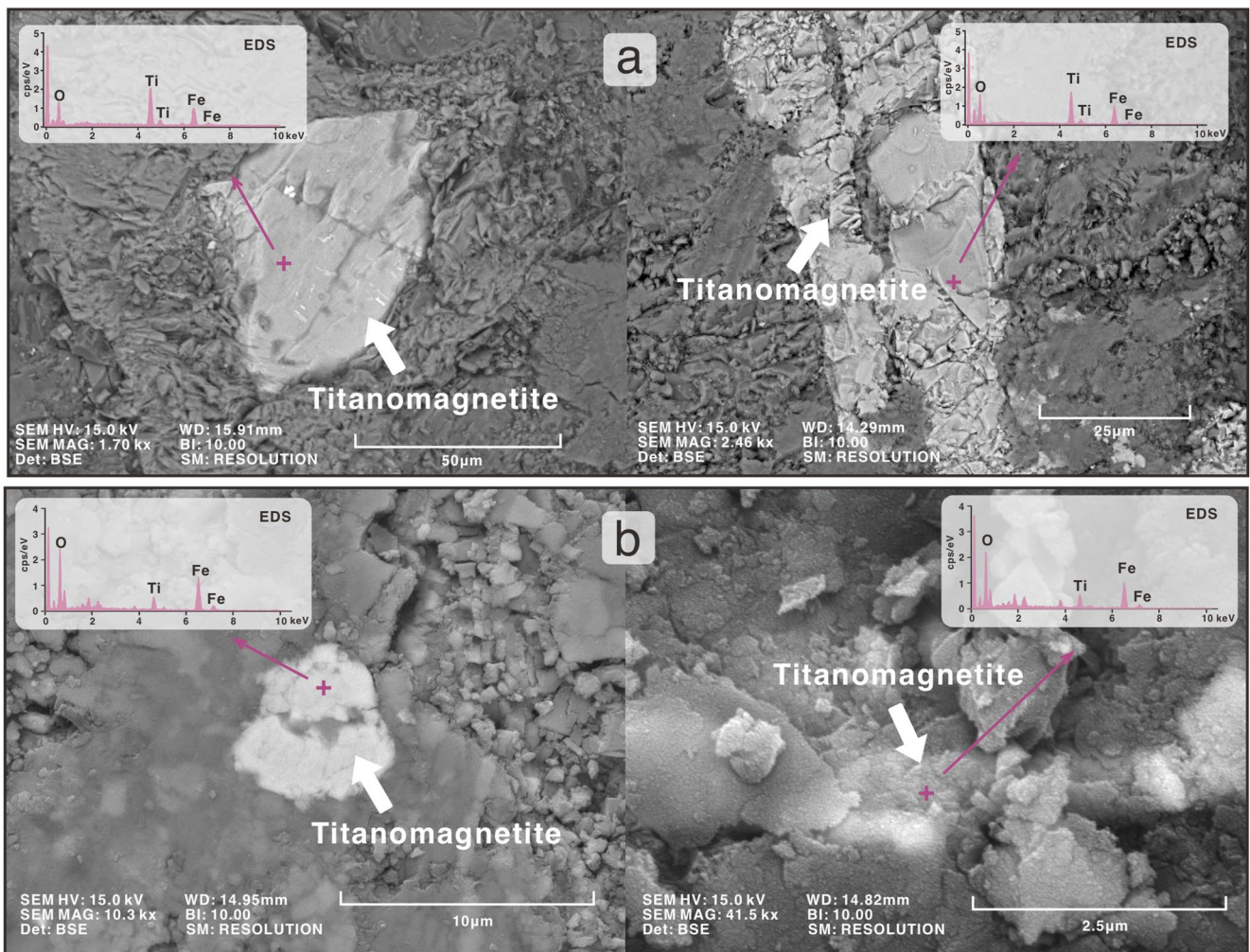


**Figure 4.** Backscattered Scanning electron microscope (SEM) images of typical magnetic minerals in the dykes from (a) North China craton (NCC) and (b) São Francisco Craton (SFC) with arrow pointing to plots of x-ray energy spectrum analysis. The purple plus signs on minerals refer to the location where x-ray energy spectrum analysis took place. The basic parameters of SEM are listed at the bottom of each image.

#### 4.4. Paleomagnetic Results

##### 4.4.1. North China Craton

As shown in Figure 5, thermal demagnetization on the dyke samples was successful. A component of viscous remagnetization with northwesterly declination and moderate positive inclination was usually removed by thermal demagnetization up to 250°C. Higher step demagnetization of most samples revealed stable characteristic remanent magnetization (ChRM) with linear decay of the demagnetization curve to the origin of vector plots (Figures 5a–5e), but only one polarity was observed.

For samples from the Dashigou dyke DSG#01 with a width of 40 m, the data were filtered to accept only sites with three or more samples contributing to the mean direction (Table 1). The  $N_{\text{dyke}}$  component which represents the ChRM component, is isolated from medium to high temperature (400°C–580°C) demagnetization with a mean direction of  $D/I = 175.1^\circ/48.8^\circ$  ( $\kappa = 89.7$ ,  $\alpha_{95} = 13.1^\circ$ ,  $N = 3$  sites) at the site level and  $D/I = 173.7^\circ/48.5^\circ$  ( $\kappa = 42.8$ ,  $\alpha_{95} = 4.8^\circ$ ,  $n = 22$  samples) at the sample level (Figure 6; Table 1). Both methods yield essentially the same results. The same data processing procedures were applied to samples from the Taohuagou dykes and Yangjiaogou dykes. The  $N_{\text{dyke}}$  component was also yielded from medium to high temperature (400°C–580°C) demagnetization. For samples from the Taohuagou dykes (THG#01 with a width of 40 m, THG#02 and THG#03, both with a width of 20 m, respectively), the mean direction of the  $N_{\text{dyke}}$  component is  $D/I = 173.4^\circ/55.9^\circ$  ( $\kappa = 104.8$ ,  $\alpha_{95} = 6.6^\circ$ ,  $N = 6$  sites) at the site level and  $D/I = 173.1^\circ/56.1^\circ$  ( $\kappa = 24.3$ ,  $\alpha_{95} = 4.6^\circ$ ,  $n = 41$  samples) at the sample level (Figure 6; Table 1). The mean direction of two Yangjiaogou dykes (YJG#01 with a width of 50 m and YJG#02 with a width of 10 m) falls at  $D/I = 194.0^\circ/65.5^\circ$  ( $\kappa = 80.0$ ,  $\alpha_{95} = 10.3^\circ$ ,  $N = 4$  sites) at the site level and  $D/I = 193.3^\circ/65.7^\circ$  ( $\kappa = 22.0$ ,  $\alpha_{95} = 6.2^\circ$ ,  $n = 26$  samples) at the sample level (Figure 6; Table 1). The combined site mean direction for the NCC dykes is  $D/I = 178.7^\circ/57.5^\circ$  ( $\kappa = 53.6$ ,  $\alpha_{95} = 5.7^\circ$ ,  $N = 13$  sites; Table 1). The mean direction of the ~30 Ma dyke NT#01 (with a width of 2 m) was  $D/I = 196.8^\circ/-64.4^\circ$  ( $\kappa = 31.6$ ,  $\alpha_{95} = 7.5^\circ$ ,  $n = 13$  samples), distinctively different from that of the 925 Ma dykes (Figure 6c).

Virtual geomagnetic poles (VGPs) were determined by initially converting the ChRM direction of each sample to the corresponding VGP, as the data in the polar space are more Fisherian (Cox, 1970). The mean VGP for each site was then averaged to determine the paleomagnetic pole and its error limit ( $A_{95}$ ). The paleomagnetic pole NC-Dykes derived from the  $N_{\text{dyke}}$  direction is located at  $-10.4^\circ\text{N}$ ,  $113.8^\circ\text{E}$ ,  $A_{95} = 7.2^\circ$  (Table 1). Averaging by regions, the VGP for Dashigou area, falls at  $-20.1^\circ\text{N}$ ,  $117.2^\circ\text{E}$  ( $A_{95} = 15.7^\circ$ ,  $N = 3$  sites), for Taohuagou area, at  $-12.0^\circ\text{N}$ ,  $117.9^\circ\text{E}$  ( $A_{95} = 7.5^\circ$ ,  $N = 6$  sites) and for Yangjiaogou area, at  $0.4^\circ\text{N}$ ,  $105.3^\circ\text{E}$  ( $A_{95} = 16.2^\circ$ ,  $N = 4$  sites). The regional averaged paleomagnetic pole is located at  $-10.6^\circ\text{N}$ ,  $113.4^\circ\text{E}$ ,  $A_{95} = 19.2^\circ$  ( $N = 3$  regions), similar to the NC-Dykes pole, but we prefer the method of averaging by sites because the mean directions are more comparable in terms of numbers of samples.

##### 4.4.2. São Francisco Craton

Thermal demagnetization removed a soft viscous overprint component and revealed stable ChRM from the SFC dyke samples. The ChRM was generally isolated in the interval of 350°C–500°C (Figure 7). The SFC samples exhibited dual polarities, forming two groups of ChRM, within which the two directions are near antipodal (Figures 7a–7e). Following the previous work in this region (Evans et al., 2016), the two groups of ChRM directions were termed “Bn” and “Br,” referring normal and reversed polarity, respectively. Paleomagnetic samples from dykes SD#04 (width ~ 1.2 m), SD#05 (width ~ 1.5 m), SD#06 (width ~ 1.7 m), and SD#07 (width ~ 40 m) yield the Bn component, with a mean direction of  $D/I = 118.1^\circ/-83.2^\circ$  ( $\kappa = 65.7$ ,  $\alpha_{95} = 8.3^\circ$ ,  $N = 6$  sites) at the site level (Figure 8a; Table 2), and  $D/I = 127.0^\circ/-83.8^\circ$  ( $\kappa = 44.2$ ,  $\alpha_{95} = 3.5^\circ$ ,  $n = 40$  samples) at the sample level (Figure 8b; Table 2). The Br component was mainly observed in Salvador dykes sites SD#01, SD#03, and SD#04, and the sill site GS#01 with a mean direction of  $D/I = 309.8^\circ/63.8^\circ$  ( $\kappa = 62.6$ ,  $\alpha_{95} = 11.7^\circ$ ,  $N = 4$  sites) at the site level (Figure 8a; Table 2) and  $D/I = 307.3^\circ/64.3^\circ$  ( $\kappa = 22.8$ ,  $\alpha_{95} = 6.5^\circ$ ,  $n = 23$  samples) at the sample level (Figure 8b; Table 2). The combination of the two directions yielded a combined mean direction Bc of  $D/I = 304.8^\circ/75.3^\circ$  ( $\kappa = 33.7$ ,  $\alpha_{95} = 8.4^\circ$ ,  $N = 10$  sites).

As listed in Tables 2 and 3, the VGP for the direction Bn calculated from the mean of the 6 sites was located at  $6.4^\circ\text{N}$ ,  $130.2^\circ\text{E}$  ( $A_{95} = 15.6^\circ$ ), and the VGP for the antipodal direction Br calculated from the mean of the 4 sites was located at  $16.5^\circ\text{N}$ ,  $288.7^\circ\text{E}$  ( $A_{95} = 19.7^\circ$ ). Combining the VGPs from the two polarity sites, the grand mean pole SF-Dykes derived from Bc was located at  $3.7^\circ\text{N}$ ,  $301.6^\circ\text{E}$  ( $A_{95} = 14.5^\circ$ ).

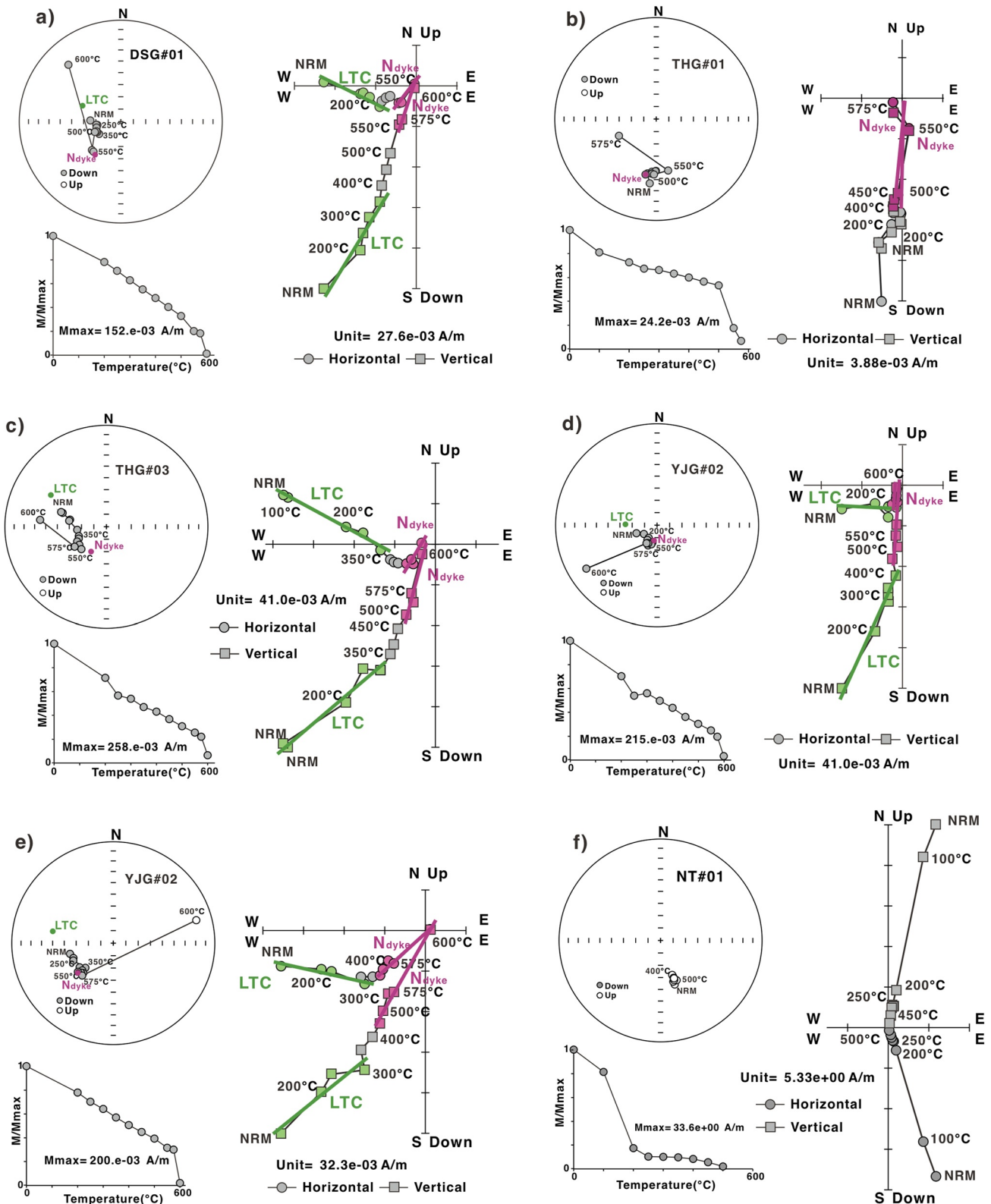


Figure 5.

**Table 1**  
Paleomagnetic Results of the 925 Ma Dyke Swarm in the NCC

Site (dyke)	Comp.	Latitude (°N)	Longitude (°E)	<i>n</i> ( <i>N</i> )	Dec (°)	Inc (°)	$\kappa$	$\alpha_{95}$ (°)	Plat (°N)	Plon (°E)	$dp/dm$ ( $A_{95}$ ) (°)
<i>Dashigou area</i>											
13n10 (DSG#01)	$N_{dyke}$	39.47	113.33	9/9	165.7	47.3	56.3	6.9	-20.8	126.7	5.8/9.0
13n11 (DSG#01)	$N_{dyke}$	39.47	113.33	7/9	173.0	44.8	46.3	9.0	-23.8	120.2	11.3/13.7
13n12 (DSG#01)	$N_{dyke}$	39.47	113.33	6/8	188.2	53.2	72.2	7.9	-16.4	106.2	7.6/11.0
<b>Mean of 3 sites</b>	$N_{dyke}$	<b>39.47</b>	<b>113.33</b>	<b>3</b>	<b>175.1</b>	<b>48.8</b>	<b>89.7</b>	<b>13.1</b>	<b>-20.1</b>	<b>117.2</b>	<b>15.7</b>
13n16 (NT#01)	$N_{Td}$	39.47	113.33	7/8	196.3	-63.4	26.8	11.9	-76.8	353.5	14.8/18.8
17n07 (NT#01)	$N_{Td}$	39.47	113.33	6/7	197.4	-65.6	32.6	11.9	-75	344.4	15.7/19.4
<b>Mean of NT#01 (sample level)</b>	$N_{Td}$	<b>39.47</b>	<b>113.33</b>	<b>13</b>	<b>196.8</b>	<b>-64.4</b>	<b>31.6</b>	<b>7.5</b>	<b>-76.0</b>	<b>349</b>	<b>9.6/10.8</b>
<i>Taohuagou area</i>											
13n04 (THG#01)	$N_{dyke}$	40.55	112.36	6/7	180.0	58.1	31.2	12.2	-10.6	112.4	13.3/18.0
13n05 (THG#01)	$N_{dyke}$	40.55	112.36	8/8	163.4	67.1	43.7	8.5	1.5	123.0	11.6/14.0
13n06 (THG#02)	$N_{dyke}$	40.53	112.38	5/8	173.6	49.3	14.3	20.9	-19.1	118.2	18.4/27.7
13n07 (THG#02)	$N_{dyke}$	40.53	112.38	7/8	167.9	58.7	67.0	7.4	-9.2	121.8	8.2/11.0
13n08 (THG#03)	$N_{dyke}$	40.53	112.38	6/7	176.6	54.9	23.8	14.0	-14.0	115.3	14.1/19.9
13n09 (THG#03)	$N_{dyke}$	40.53	112.38	9/9	175.4	46.8	20.3	11.7	-21.3	116.8	9.7/15.1
<b>Mean of 6 sites</b>	$N_{dyke}$	<b>40.53</b>	<b>112.38</b>	<b>6</b>	<b>173.4</b>	<b>55.9</b>	<b>104.8</b>	<b>6.6</b>	<b>-12.0</b>	<b>117.9</b>	<b>7.5</b>
17n06 (Country rock)	$N_{Cr}$	40.53	112.38	6/7	54.6	-11.0	73.0	7.9	22.0	231.3	4.1/8/0
<i>Yangjiaogou area</i>											
13n01 (YJG#01)	$N_{dyke}$	40.70	114.37	8/9	194.6	59.9	32.8	9.8	-7.5	103.3	11.2/14.8
13n02 (YJG#01)	$N_{dyke}$	40.70	114.37	6/7	172.6	65.5	12.4	19.8	-1.3	119.3	26.1/32.1
13n03 (YJG#02)	$N_{dyke}$	40.70	114.37	8/8	187.8	66.5	27.8	10.7	0.0	109.3	14.5/17.6
17n01 (YJG#02)	$N_{dyke}$	40.70	114.37	5/8	222.0	66.1	37.3	12.7	6.5	87.8	17/20.8
<b>Mean of 4 sites</b>	$N_{dyke}$	<b>40.70</b>	<b>114.37</b>	<b>4</b>	<b>194.0</b>	<b>65.5</b>	<b>80.0</b>	<b>10.3</b>	<b>0.4</b>	<b>105.3</b>	<b>16.2</b>
<b>Mean of 925 Ma dykes (site level)</b>	$N_{dyke}$	/	/	<b>13</b>	<b>178.7</b>	<b>57.5</b>	<b>53.6</b>	<b>5.7</b>	<b>-10.4</b>	<b>113.8</b>	<b>7.2</b>
<b>Mean of 925 Ma dykes (sample level)</b>	$N_{dyke}$	/	/	<b>90</b>	<b>177.8</b>	<b>57.2</b>	<b>22.0</b>	<b>3.3</b>	<b>-10.2</b>	<b>114.5</b>	<b>4.2</b>
<b>Mean of 925 Ma dykes (dyke/intrusion level)</b>	$N_{dyke}$	/	/	<b>6</b>	<b>179.1</b>	<b>58.2</b>	<b>70.6</b>	<b>8.0</b>	<b>-9.9</b>	<b>113.4</b>	<b>10.0</b>

Note. Comp., stable component isolated from demagnetization curves;  $N_{dyke}$ , the ChRM component of 925 Ma dykes in NCC;  $N_{Td}$ , the ChRM component of ~30 Ma dyke NT#01;  $N_{Cr}$ , the component of unbaked country rocks of dyke THG#01; *n*(*N*), number of samples (sites) for statistic; Dec, declination; Inc, inclination;  $\kappa$ , Fisher precision parameter of the mean;  $\alpha_{95}/A_{95}$ , radius of circle of 95% confidence about the mean direction/pole; Plat/Plon, latitude/longitude of VGP;  $dm/dp$ , semi-axes of elliptical error around the pole at a probability of 95%. Bolded data are used for Figures 6, 8, 10 and 11, and mean pole calculation.

## 5. Discussion

### 5.1. Origin and Stability of the ChRM

As with any paleomagnetic study, it is critical to establish the reliability of the paleomagnetic pole and ensure the ChRM mentioned above is the primary remanent magnetization.

The ChRM isolated from the NCC samples is rather stable. We performed a baked contact test on dyke THG#01 of the Taohuagou dykes. Samples were collected from two sites of the ~1.95 Ga porphyritic garnet granites that have been intruded by THG#01 (40 m wide), in which one site of baked rocks lies approximately 0.35 m to the

**Figure 5.** Stepwise thermal demagnetization results of representative samples from the North China craton (NCC) (shown in geographic coordinates): (a) DSG#01, (b) THG#01, (c) THG#03, (d–e) YJG#02, and (f) NT#01. “LTC” (green line) stands for the low temperature component, and “ $N_{dyke}$ ” means the characteristic remanent magnetization (ChRM) component of the 925 Ma dykes in the NCC. Circles represent the horizontal component in the orthogonal vector diagram and lower hemisphere projections for the stereonets, while boxes represent the vertical components/upper hemisphere projections. The colored straight lines represent the points involved in the principal component analysis (PCA) and the fitted direction, respectively.

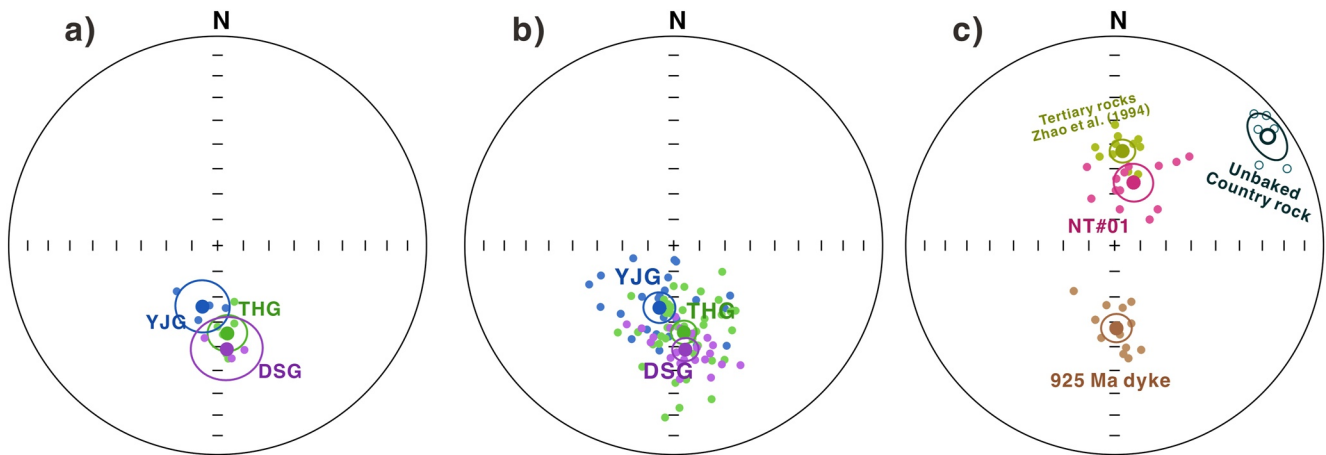


**Figure 6.** Equal area projections of (a) site-mean characteristic remanent magnetization (ChRM) directions from 925 Ma dykes in the NCC. YJG: Yangjiaogou dykes (blue), THG: Taohuagou dykes (green), DSG: Dashigou dykes (purple); (b) mean ChRM directions of the 925 Ma dykes in NCC at sample level (the colors and abbreviations indicate the same areas as in Figure 6a); (c) site-mean ChRM directions: the 925 Ma dykes in NCC (brown); mean directions from unbaked country rocks of THG#01 (dark green) at sample level; inverted directions from ~30 Ma dyke NT#01 at sample level (magenta), and results of Tertiary rocks at site level (light green) from X. Zhao et al. (1994). Open and full circles represent upper and lower hemisphere projections, respectively.

contact boundary, and the other site was unbaked rocks lying approximately 30 m away from the main dyke. The ChRM of the unbaked rocks ( $D/I = 54.6^\circ/-11.0^\circ$ ,  $\kappa = 73.0$ ,  $\alpha_{95} = 7.9^\circ$ ,  $n = 6$  samples) exhibited a distinct direction from that of THG#01, but close to the expected direction ( $D/I = 57.2^\circ/-11.9^\circ$ ,  $\alpha_{95} = 15.2^\circ$ ) of Paleoproterozoic pole (A1) of the NCC at this site (Figure 9a; J. Zhang & Piper, 1994). For the baked rock, although the declinations of the sample are rather scatter, the inclination values are similar to that of the THG#01 and have the same polarity (Figure 9a). Although the above does not refer to a strictly positive baked contact test, the direction trends among these sites nevertheless suggest a baked effects and ruling out a late remagnetization of the region since the emplacement of the Taohuagou dykes. Similarly, the ~30 Ma dyke NT#01 lying approximately 350 m west of the Dashigou dyke DSG#01 in Hebei Province also yielded a stable ChRM direction ( $D/I = 196.8^\circ/-64.4^\circ$ ,  $\kappa = 31.6$ ,  $\alpha_{95} = 7.5^\circ$ ,  $n = 13$  samples) that is completely different from that of ChRM  $N_{\text{dyke}}$  (Figure 6c). The excellent agreement between the corresponding pole of this 30 Ma dyke and the expected Tertiary pole for the NCC (X. Zhao et al., 1994) provides additional support for the argument that no significant tectonic tilt occurred in the sampling region at least since 30 Ma ago. In addition, the  $A_{95}$  values of the corresponding NCC dyke poles (Table 1) fall within the N-dependent confidence interval (6.1, 16.3, for  $N = 13$  sites; 2.8, 4.8, for  $N = 90$  samples), implying that the paleopoles have averaged out paleosecular variation (Deenen et al., 2011).

To sum up, because the final demagnetization curves were linear, the mean directions of widely distributed localities in three provinces exhibited internal consistency, the baked contact tests produced positive results, and magnetization is carried by low-titanium titanomagnetites, which are capable of preserving early remanent magnetization over a long period of time, we conclude that the ChRMs of the 925 Ma dykes from the NCC represents records of the paleomagnetic field close in age to the emplacement of these 925 Ma dykes and are suitable for calculating the 925 Ma poles for the NCC.

The demagnetization of the SFC samples is relatively straightforward (Figure 7). The ChRM component was mostly of normal polarity. At a few sites, a reversed ChRM component was also observed, with directions roughly antiparallel to the majority of the normal ChRM directions, indicating that paleosecular variation may have been averaged out by these dykes. The corresponding means of  $B_r$  and  $B_n$ , however, did not pass the reversal test of McFadden and McElhinny (1990), differing from anti-parallel at greater than 95% confidence level ( $\gamma_o = 19.5^\circ > \gamma_c = 12.8^\circ$ ). It is worth mentioning that clearly defined ChRM directions of dual polarity were obtained from two samples in site dyke SD#05 within a distance of 1.5 m (Figure 9b), indicating at least two pulses of emplacement have been occurred at this dyke site. Several field checks were also performed to test the stability of the ChRMs of the Salvador dykes, including a baked contact test (Figure 9c). Six samples were drilled from the Paleoproterozoic granulites intruded by dyke SD#06. The direction of two unbaked samples collected approximately 1.0 m west of the dyke differed from that of the host rock, close to the component isolated from the supposed Paleoproterozoic rock samples (Figure 9c;  $S_{\text{MN}}$ ,  $D/I = 294.9^\circ/-42.5^\circ$ ,  $\alpha_{95} = 11.3^\circ$  in D'Agrella-Filho

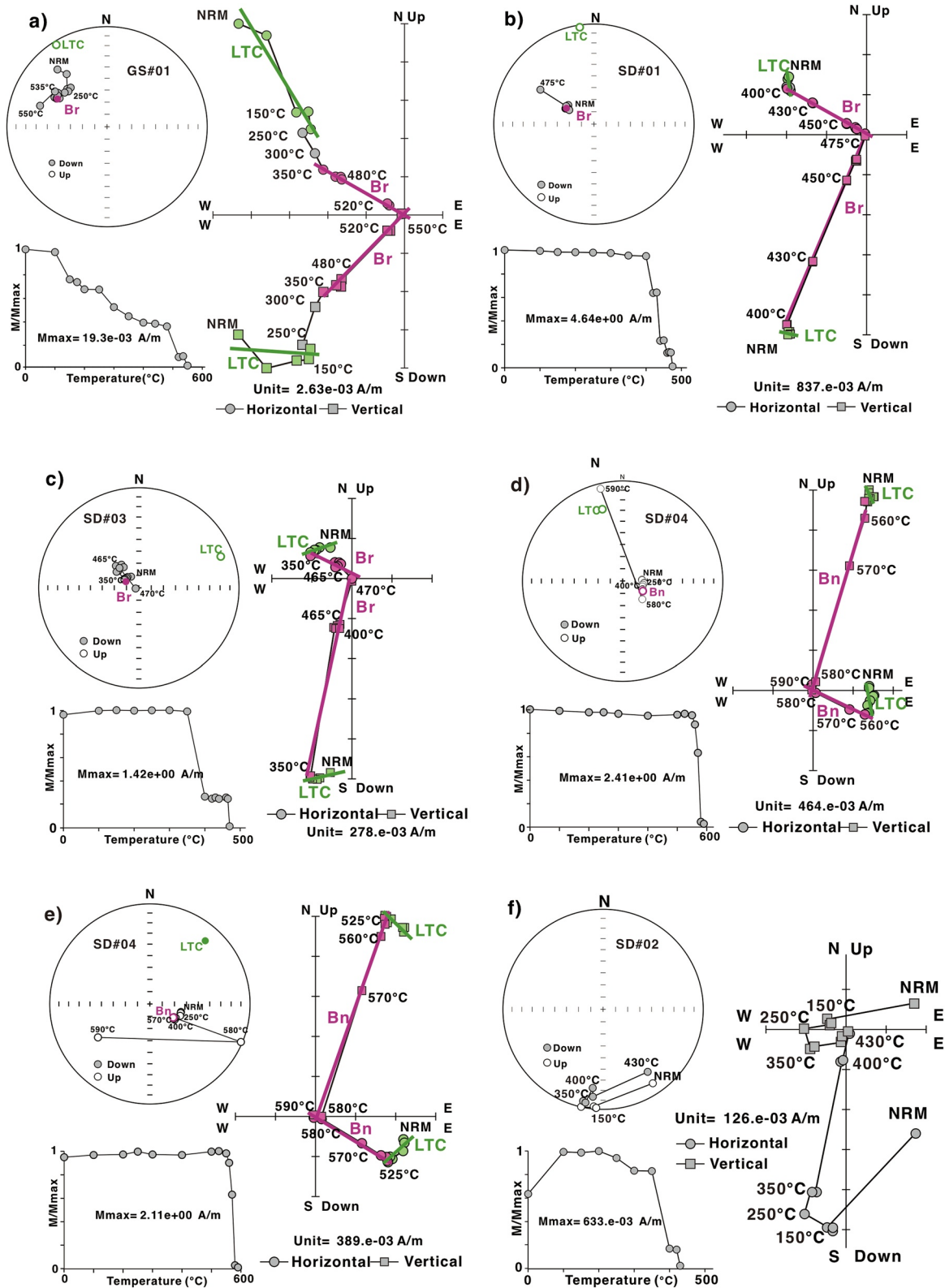


**Figure 7.** Stepwise thermal demagnetization results of representative samples from the São Francisco Craton (SFC) (shown in geographic coordinates): (a) GS#01, (b) SD#01, (c) SD#03, (d–e) SD#04 and (f) SD#02. "Bn" and "Br" mean normal and reversed characteristic remanent magnetization (ChRM) components of the ~930–925 Ma dykes and sill in the SFC. Other symbols are same as those in Figure 5.

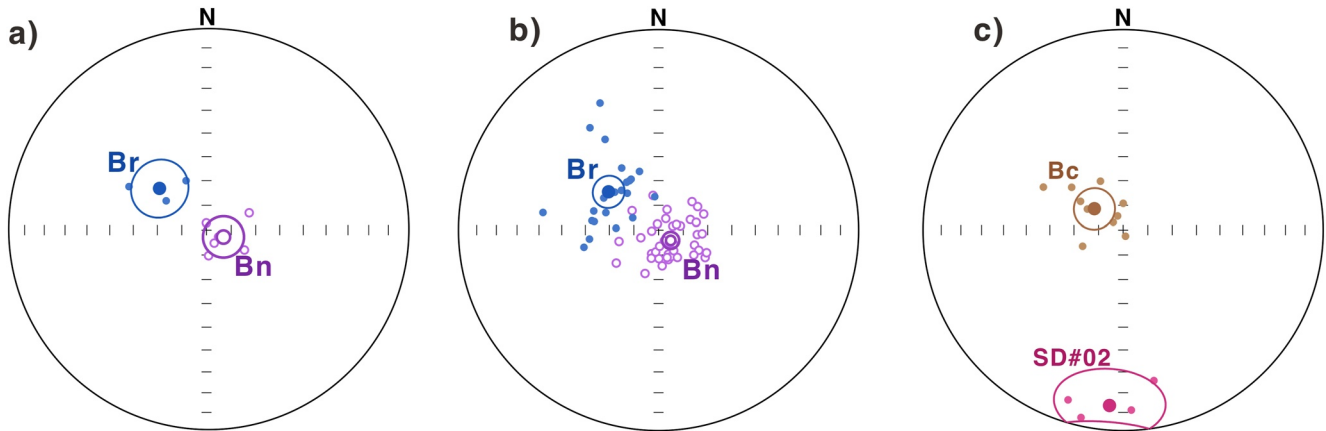


**Figure 8.** Equal area projections of (a) site-mean characteristic remanent magnetization (ChRM) directions from the Salvador dykes (Br component: blue and the Bn: purple); (b) mean ChRM directions of Salvador dykes in São Francisco Craton (SFC) at sample level (the colors correspond to the same areas as in Figure 8a); (c) combined site-mean ChRM directions (Bc) from the Salvador dykes in SFC (brown) and the mean directions from dyke SD#02 (magenta) at the sample level.

et al., 2004). On the contrary, the direction of ChRM from three baked samples collected approximately 0.1 m from dyke SD#06 was quite consistent with that of the dyke SD#06 (Figure 9c). In addition, samples from dyke SD#02 yielded mean direction at  $D/I = 184.4^\circ/13.3^\circ$ ,  $\kappa = 27.5$ ,  $\alpha_{95} = 17.8^\circ$ ,  $n = 4$  samples (Figures 8c, Table 2), which is different from that of dyke SD#01 cut by SD#02, offering additional support for the primary magnetization of the 925 Ma dyke.

**Table 2**  
Paleomagnetic Results of the ~930–925 Ma Dykes and Sill in the SFC

Site (dyke/sill)	Comp.	Latitude (°S)	Longitude (°W)	$n(N)$	Dec (°)	Inc (°)	$\kappa$	$\alpha_{95}$ (°)	Plat (°N)	Plon (°E)	$dp/dm$ ( $A_{95}$ ) (°)
17s06 (GS#01)	Br	11.418	42.551	5/7	298.2	52.7	9.1	26.7	16.2	267.4	25.4/36.9
19s01 (SD#01)	Br	13.014	38.476	6/9	309.6	62.7	31.3	12.2	16.8	286.2	14.9/19.1
19s03 (SD#03)	Br	13.014	38.476	9/9	303.9	69.1	59.3	6.7	8.7	290.9	9.8/11.5
19s04A (SD#05)	Br	13.011	38.482	3/8	335.0	68.1	78.9	14.0	22.3	304.9	19.7/23.5
<b>Mean of 4 sites</b>	<b>Br</b>	/	/	<b>4</b>	<b>309.8</b>	<b>63.8</b>	<b>62.5</b>	<b>11.7</b>	<b>16.5</b>	<b>288.7</b>	<b>19.7</b>
17s07 (SD#04)	Bn	13.014	38.476	6/9	120.3	-73.2	106.6	6.5	-3.5	115.3	10.4/11.7
19s04B (SD#05)	Bn	13.011	38.482	4/8	68.4	-72.3	182.0	6.8	22.5	108.8	10.7/12.1
19s06 (SD#06)	Bn	13.011	38.482	7/8	338.4	-87.4	52.4	8.4	17.8	143.5	16.7/16.8
19s07 (SD#07)	Bn	13.011	38.482	10/10	128.4	-84.9	45.2	7.3	6.7	133.6	14.2/14.4
19s08 (SD#07)	Bn	13.011	38.482	7/8	180.3	-79.2	86.8	6.5	-7.9	141.6	11.8/12.4
19s09 (SD#07)	Bn	13.011	38.482	6/8	158.6	-83.9	208.1	4.7	1.8	137.1	9/9.2
<b>Mean of 6 sites</b>	<b>Bn</b>	/	/	<b>6</b>	<b>118.1</b>	<b>-83.2</b>	<b>65.7</b>	<b>8.3</b>	<b>6.4</b>	<b>130.2</b>	<b>15.6</b>
19s02 (SD#02)	$B_{Yd}$	13.014	38.476	4/9	184.4	13.3	27.5	17.8	-82.4	176.9	9.3/18.2
19s05A (baked country rock)	$B_{bcr}$	13.011	38.482	3/6	64.1	-70.7	33.7	21.6	25.4	106.7	32.5/37.4
19s05B (unbaked country rock)	$B_{ucr}$	13.011	38.482	2/6	292.2	-54.7	91.6	26.4	25.5	198.5	26.4/37.3
<b>Mean of 925 Ma dykes (site level)</b>	<b>Bc</b>	/	/	<b>10</b>	<b>304.8</b>	<b>75.3</b>	<b>33.7</b>	<b>8.4</b>	<b>3.7</b>	<b>301.6</b>	<b>14.5</b>
<b>Mean of 925 Ma dykes (sample level)</b>	<b>Bc</b>	/	/	<b>63</b>	<b>307.2</b>	<b>76.8</b>	<b>23.3</b>	<b>3.8</b>	<b>1.7</b>	<b>303.1</b>	<b>6.2</b>
<b>Mean of 925 Ma dykes (dyke/intrusion level)</b>	<b>Bc</b>	/	/	<b>7</b>	<b>303.5</b>	<b>72.9</b>	<b>37.0</b>	<b>10.1</b>	<b>4.2</b>	<b>296.9</b>	<b>16.9</b>

Note. Comp., stable component isolated from demagnetization curves; Bn and Br, the normal and reversed ChRM components of 925 Ma dykes in SFC;  $B_{Yd}$ , the component of dyke SD#02 cutting SD#01;  $B_{bcr}$ , the component of baked country rocks intruded by SD#06;  $B_{ucr}$ , the component of unbaked country rocks intruded by SD#06;  $n(N)$ , number of samples (sites) for statistic; Dec, declination; Inc, inclination;  $\kappa$ , Fisher precision parameter of the mean;  $\alpha_{95}/A_{95}$ , radius of circle of 95% confidence about the mean direction/pole; Plat/Plon, latitude/longitude of VGP;  $dm/dp$ , semi-axes of elliptical error around the pole at a probability of 95%. Bolded data are used for Figures 6, 8, 10 and 11, and mean pole calculation.

Inverting the site means of negative inclination to positive and combining site-means, the corresponding paleomagnetic pole SF-Dykes agrees well with that of previous studies on the 925 Ma dykes in the SFC (Figure 10; Table 3; D'Agrella-Filho et al., 1990, 2004; Evans et al., 2016), which is expected as the studied rocks are essentially the same. The  $A_{95}$  value of our new SFC pole (Table 2) also falls within the  $A_{95}$  envelop (6.8, 19.2,  $N = 10$  sites; 3.2, 6.0,  $N = 63$  samples) of Deenen et al. (2011), implying that the confidence limit of the paleopole is consistent with paleosecular variation (Deenen et al., 2011). Collectively, the results of this study as well as those from previous studies offer a reliable paleomagnetic pole for the SFC during 925 Ma.

In summary, the paleomagnetic results of the 925 Ma dykes from both NCC and SFC reveal both overprinted and primary components. The low temperature component is secondary magnetization imposed mainly in recent times. The ChRM component is interpreted to be primary or near-primary remanent magnetization, as shown by the positive baked contact tests and dual polarity of the SFC dykes, indicating the absence of regional overprint events that reset the magnetization of the 925 Ma dykes. The 925 Ma poles also differ from younger NCC and SFC poles, consistent with a primary origin.

## 5.2. Paleogeographic Reconstruction of the NCC and SFC in Rodinia

Reconstructing paleogeography not only depends on geologic records but also relies critically on paleomagnetic poles for various continents to confirm their paleo-positions.

The interval from the late Mesoproterozoic to early Neoproterozoic is generally considered as a critical time for the amalgamation of Rodinia. However, recent reassessments of the radiometric dates from the NCC suggest that a large portion of high-quality Precambrian paleomagnetic poles of the NCC are aged older than  $\sim 1.35$  Ga (Chen et al., 2013; Halls et al., 2000; Xu et al., 2014; S. Zhang et al., 2012). The dominantly negative inclination of the ChRM components found in these studies would indicate that the field in these time periods was mainly reversed. Two suggestions have been tendered concerning the locations of the NCC during the time period of

**Table 3**  
Paleomagnetic Poles of NCC, SFC, Baltica and Laurentia Used for Paleogeographic Reconstruction

Pole	Age (Ma)	Rock type	Plat (°N)	Plon (°E)	dp/dm $A_{95}$ (°)	$Q$	Reference
<i>North China Craton (NCC) (Euler's Rotation: 40.2, 26.5, -178.9, rotated to present SFC position)</i>							
NC-Dykes	924 ± 3.7	925 Ma dykes in NCC	-10.4	113.8	7.2	5	This study
NC-Dykes (dyke/intrusion level)	924 ± 3.7	925 Ma dykes in NCC	-9.9	113.4	10.0	5	This study
XS2	890 ± 14	~890 Ma Sills in Huaibei region	52.6	330.0	5.3	7	Fu et al. (2015)
XS1	925 ± 10	~925 Ma Sill in Huaibei region (VGP)	-30.9	136.2	2.4/4.0	3	Fu et al. (2015)
WS	1,121-890	Wangshan Formation	26.1	320.3	5.2	4	Fu et al. (2015)
NF	<1,077	Nanfen Formation	-16.5	121.1	8.8/13.0	4	Lin (1984)
BNFc	>945	Middle Member of Nanfen Formation	-11.2	127.7	8.5	4	H. Zhao et al. (2020)
NC930	~945-920	Sills	-28.2	141.9	10.4	6	H. Zhao et al. (2020)
<i>São Francisco Craton (SFC) (Euler's Rotation: -11.4, -44.4, -123.2, rotated to present Laurentia position)</i>							
SF-Dykes	~930-925	~930-925 Ma dykes and sill in SFC	3.7	301.6	14.5	5	This study
SF-Dykes (dyke/intrusion level)	~930-925	~930-925 Ma dykes and sill in SFC	4.2	296.9	16.9	5	This study
Ba	925-920	Bahia-coastal dykes	-7.0	286.0	6.0	6	Evans et al. (2016)
Ic	ca.925?	Itaju do Colônia dykes -C	-7.7	291.0	9.8	4	D'Agrella et al. (1990)
<i>Laurentia (Euler's Rotation: 45.31, 162.32, 174.19)</i>							
Ld	900	Nankoweap Formation	-8	161.1	2.4	4	Elston et al. (2002)
<i>Baltica (Euler's Rotation: 81.5, 250.0, -50.0, rotated to present Laurentia position)</i>							
SSD	946-935	Mean 946-935 Ma Baltica pole	1	61	6.8	7	Elming et al. (2014)

Note. Plat/Plon, latitude/longitude of VGP; dm/dp, semi-axes of elliptical error around the pole at a probability of 95%;  $A_{95}$ , radius of circle of 95% confidence about the mean pole;  $Q$ , number of the  $Q$ -factors has been met (Van der Voo, 1990).

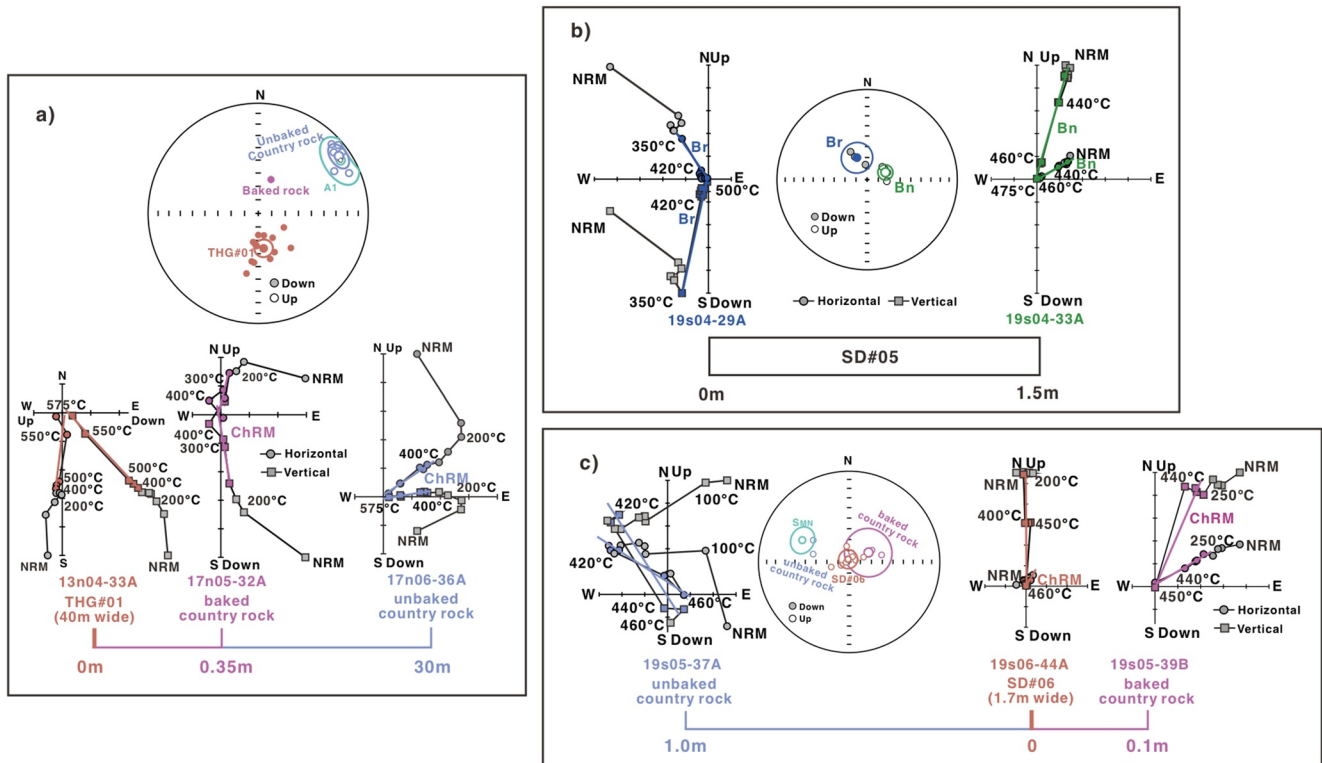


**Figure 9.** Results of positive baked contact tests in this study (symbols and color lines are same as those of Figure 5). (a) A partially positive baked contact test of dyke THG#01 (~40 m wide) in the Taohuagou area of North China craton (NCC). Although the baked country rocks do not yield a stable characteristic remanent magnetization (ChRM), the direction of unbaked Paleoproterozoic country rocks (30 m from the main dyke) differs from that of THG#01, and is close to the Paleoproterozoic direction A1 reported in (j) Zhang & Piper. (1994). (b) Dyke SD#05 in the Salvador area of SFC. The dyke yielded distinct directions with a maximum interval of 1.5 m, indicating two pluses of dyke emplacement and the absence of regional events resetting the remanent magnetization of the dyke sites. (c) A positive baked contact test of the dyke SD#06 (1.7 m wide) in Salvador. The baked country rocks 0.1 m east of the dyke have a similar direction with dyke SD#06, and unbaked Paleoproterozoic granulites about 1.0 m west of dyke yield different directions from component  $B_n$ , but the directions are close to component  $S_{MN}$  from Paleoproterozoic metamorphic samples (D'Agrella-Filho et al., 2004).

1.78–1.35 Ga with little explanation of underlying rationale (a) northern hemisphere (i.e., Chen et al., 2013; S. Zhang et al., 2012): and (b) southern hemisphere (i.e., Halls et al., 2000; Xu et al., 2014).

In recent years, several Neoproterozoic paleomagnetic poles relevant to this study have been reported for the NCC (Fu et al., 2015; H. Zhao et al., 2020). These paleopoles (Table 3) consist of pole NC930 (from ca. 945–920 Ma sills), pole BNFc (from ~945 to 920 Ma calcareous mudstone and limestone in the middle part of the Nanfen Formation), pole XS1 (from ~925 Ma sills), pole XS2 (from ~890 Ma sills), and pole WS (from 950 to 890 Ma carbonates of the Wangshan Formation). Among these poles, pole NC930 was derived from three sills dated at ca. 945 Ma and one at ca. 920 Ma from eastern NCC, with positive results of baked-contact test and presence of both polarities (Fu et al., 2015, H. Zhao et al., 2020). Poles BNFc and WS were obtained from sedimentary rocks that are approximately coeval to our 925 Ma dykes (Fu et al., 2015; H. Zhao et al., 2020). Despite the differences in pole positions, the paleolatitudes inferred from poles NC930, BNFc and WS are similar with ours. This reinforces the interpretation that the ChRM component found in this study is possibly primary.

The predominantly positive inclination of our 925 Ma dyke site direction from the NCC can be interpreted to indicate that the NCC lay either in the northern hemisphere during a mainly normal polarity period or in the southern hemisphere during a mainly reversed polarity period. It is then not clear whether the corresponding paleopole from the 925 Ma dyke in the NCC is north or south pole because the polarity of the field associated with the sample directions is not known and the gaps in the apparent polar wander path (APWP) for the NCC during Proterozoic–Paleozoic time are large. Thus, it is impossible to extrapolate back in time from paleomagnetic data to constrain the polarity for the Neoproterozoic.

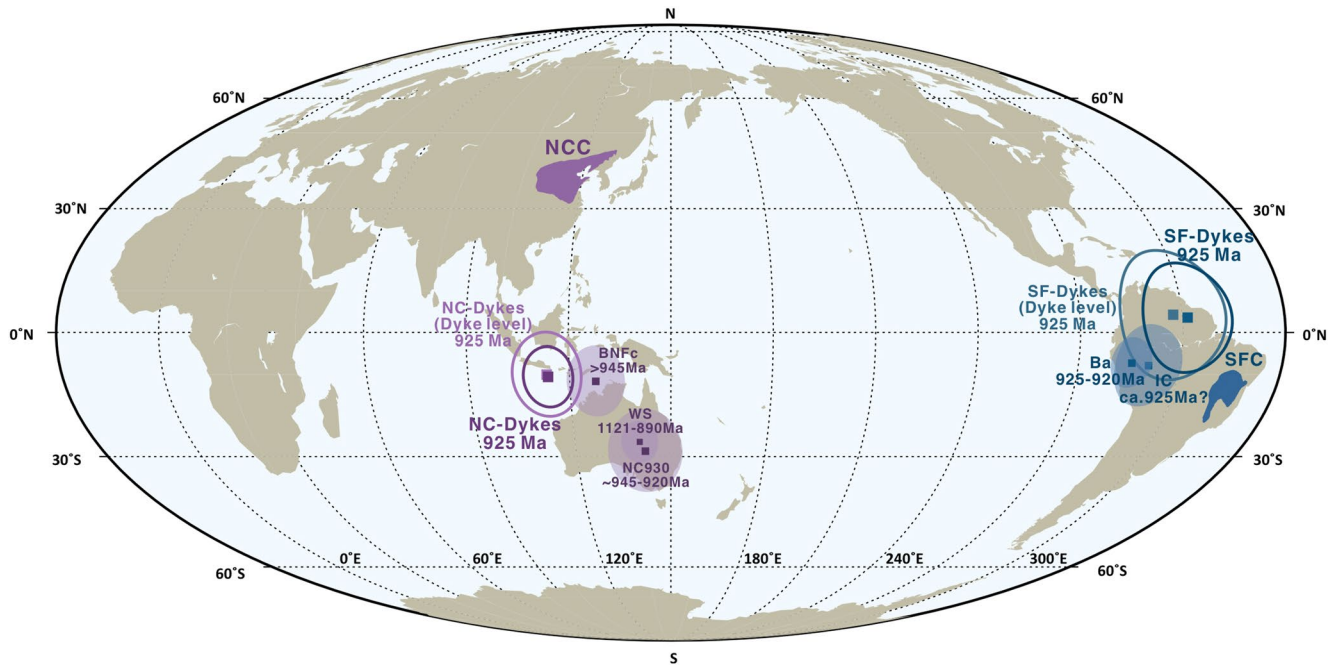


**Figure 10.** Early Neoproterozoic paleomagnetic poles with confidence circles ( $A_{95}$ ) in present coordinates, illustrating the new poles NC-Dykes (purple) and SF-Dykes (blue) obtained in this study. Several paleomagnetic poles of the North China craton (NCC) (purple) and São Francisco Craton (SFC) (blue) from previous studies (Table 3; D'Agrella-Filho et al., 1990; Evans et al., 2016; Fu et al., 2015; H. Zhao et al., 2020) are also shown. Cratons and their poles are matched in color. Note: Pole WS is plotted as south pole from the original study (Fu et al., 2015).

The mean direction corresponding to the pole WS is at  $D/I = 337.2/-44.1^\circ$  ( $\kappa = 116.2$ ,  $\alpha_{95} = 4.8^\circ$ ,  $N = 9$  sites), which is antipodal to the ChRM of this study. The pole WS passed a fold test, suggesting that the ChRM suffered little or no post-folding deformation and remagnetization. If we take liberty with the polarity designation of the pole WS in Fu et al. (2015) and assume the generalization was true that the earth's geomagnetic field was mainly reversed during the late Mesoproterozoic to early Neoproterozoic, as mentioned above, then the NCC would be placed in the southern hemisphere. This polarity choice not only is mutually consistent with the same polarity of coeval paleopoles from the SFC and the geologic match of the same age mafic dykes on both cratons, but also has the effects of maintaining and a more consistent paleo-orientation relationship for the NCC between 925 Ma and early Paleozoic in which NCC was believed as part of Gondwana in the southern hemisphere (Huang et al., 1999; G. Zhao et al., 2018). Burrett et al. (1990) also suggested that Cambrian and Early Ordovician fauna from North China are similar to those of Australia, which is consistent with the paleomagnetically inferred southern latitudes and suggests that NCC may have been part of Gondwana in Early Paleozoic time.

As shown in Figure 10, the new paleomagnetic pole (NC-Dykes) obtained from this study lies adjacent to the pole BNFc with a 95% confidence circle overlapped but maintains a certain distance with other poles (poles NC930 and WS). It is noteworthy that some of the sites investigated by Fu et al. (2015) and H. Zhao et al. (2020) are very close to the strike-slip Tanlu fault zone, suggesting problems of structural disturbance because the close proximity to the Tanlu fault zone cannot be precluded.

The age of NC-Dykes is well constrained, with rigorous chronology constraints including U-Pb baddeleyite ages of  $924.0 \pm 3.7$  Ma for the Dashigou dykes,  $921.8 \pm 2.6$  Ma for the Yangjiaogou dykes and  $925.8 \pm 1.7$  Ma for the Taohuagou dykes. Considering the uncertainty in the age of previous paleopoles (poles WS, BNFc and other existing poles of uncertain age in Table 3), our new paleomagnetic pole NC-Dykes is reasonably more representative of the NCC for the paleogeographic reconstruction during 925 Ma.

The scarcity of reliable paleomagnetic data of the SFC during the Mesoproterozoic limits the construction of a reliable APW path of SFC from the Mesoproterozoic to the early Neoproterozoic. Recent progresses in geochronology greatly have improved the geologic and tectonic records of Laurentia, Baltica, and Amazonia, as well as Precambrian paleomagnetic poles from the three cratons, which were sutured along collisional orogenic belts during 1.08–0.98 Ga

(Cawood et al., 2016). These cratons have also become backbone cratons for developing paleogeographic models of the Rodinia. The classic Rodinia model suggests that the SFC lied on the west of Amazonia for the future collision of two cratons along the late Neoproterozoic to Cambrian Brasiliano orogenic belt (Li et al., 2008; G. Zhao et al., 2018). The paleogeographic configuration between the SFC and Amazonia is further constrained by geological records of ancient ocean basins in the early Neoproterozoic (Cordani et al., 2009) and the absence of collision-related rock units at that time (Merdith et al., 2017), indicating a large ocean separating the SFC and Amazonia.

As mentioned, the possible paleogeographic connection of the NCC and SFC during 925 Ma has been suggested in recent papers based on geologic records (Caxito et al., 2020; Cederberg et al., 2016; Chaves et al., 2019; Peng, Bleeker, et al., 2011), although the corresponding models widely varied from each other due to the lack of coeval paleomagnetic investigations. To combine our current paleomagnetic knowledge on both NCC and SFC, we have attempted the paleogeographic reconstruction of the two cratons during 925 Ma in this study (Figure 11a), according to the mean paleopoles in Table 3. In the proposed reconstruction, both cratons are placed southwest of Laurentia in moderate to high paleolatitudes, allowing a possibility of paleogeographic connection between the NCC and SFC at 925 Ma. The positions of other nucleus blocks of Rodinia relative to the SFC were placed according to the classic models (Li et al., 2008; Merdith et al., 2017).

Despite the paleolatitude of the NCC derived from the new paleopole NC-Dykes of NCC is similar to that of SFC, the NCC and SFC could have possibly moved along lines of equal latitude because the paleolongitudes are unconstrained. Thus, although we are not in a position to uniquely resolve this problem, we call attention on the reported results of provenance and basin history analysis.

Sun et al. (2020) have reported that characteristic spectrum of detrital zircon ages from Tonian Basins in the NCC may have middle to late Mesoproterozoic provenance from southwest Congo Craton. The Xuhuai rift system of the NCC, together with the upper Espinhaço rift system of the SFC, most likely comprise a unified rift system during 0.9–1.1 Ga (Peng, Bleeker, et al., 2011; Sun et al., 2020). These geologic observations and inferences are readily explained if a geographic proximity of the two cratons already existed.

In recent years, an increasing number of studies have reported that the initial geometry of dykes and magma flow can be constrained by AMS (magnetic fabrics) results (e.g., Koopmans et al., 2022). AMS data obtained from this study provide additional support for the geographic link: the 900–925 Ma mafic dykes are mainly distributed in the NCC, SFC and Congo craton, of which the 925 Ma dykes in the NCC and SFC exhibit similar geochemical and geometry characteristics (Ernst et al., 2008; Peng, Bleeker, et al., 2011). Excluding the NCC, the other two cratons have been placed southwest of Laurentia, to form the nucleus of west Gondwana (e.g., Merdith et al., 2017).

The 925 Ma dykes in the NCC exhibit an overall radiating geometry trending  $305^{\circ}$ – $010^{\circ}$  (Peng, Bleeker, et al., 2011). This pattern is speculated to correspond to single radiating dyke system together with coeval dykes in the SFC and Congo Craton (Chaves et al., 2019; Su et al., 2021). The AMS results obtained in this study corroborate this speculation: according to the  $K_{\max}$ – $K_{\text{int}}$  plane, the dykes in both NCC and SFC were in lateral flow with the NW-SE trend during emplacement (Figures S2 and S3 in Supporting Information S1). The characteristics of the emplacement mode strengthen the hypothesis that the dykes in the two cratons may have originated from the same magmatic plumbing system and formed a radiating dyke swarm (Figure 11b). Thus, the close agreement between the dyke geometry offers a coherent picture of possible paleogeographic connection in which the NCC was located northwest of the SFC.

Together, these correlatable geologic and rock magnetic data indicate that NCC and SFC are very likely two ancient cratons with a geographic connection. This configuration between the NCC and SFC is more contingent with their involvements in subsequent assembly of Gondwana. The southern hemisphere paleo-position of the NCC is consistent with other paleogeographic models that place the NCC as part of Gondwana in the early Paleozoic (Huang et al., 1999, 2000, 2018; G. Zhao et al., 2018). For the SFC, its relationship with the Amazonia is consistent with the classic model (Li et al., 2008; G. Zhao et al., 2018) that the SFC was located on the west of Amazonia before its collision with Amazonia in late Neoproterozoic-Cambrian time.

## 6. Conclusion

This investigation, integrating paleomagnetic and rock magnetic studies and scanning electron microscope analysis, was conducted on coeval dykes with a well-constrained age of 925 Ma in the North China and São Francisco cratons.

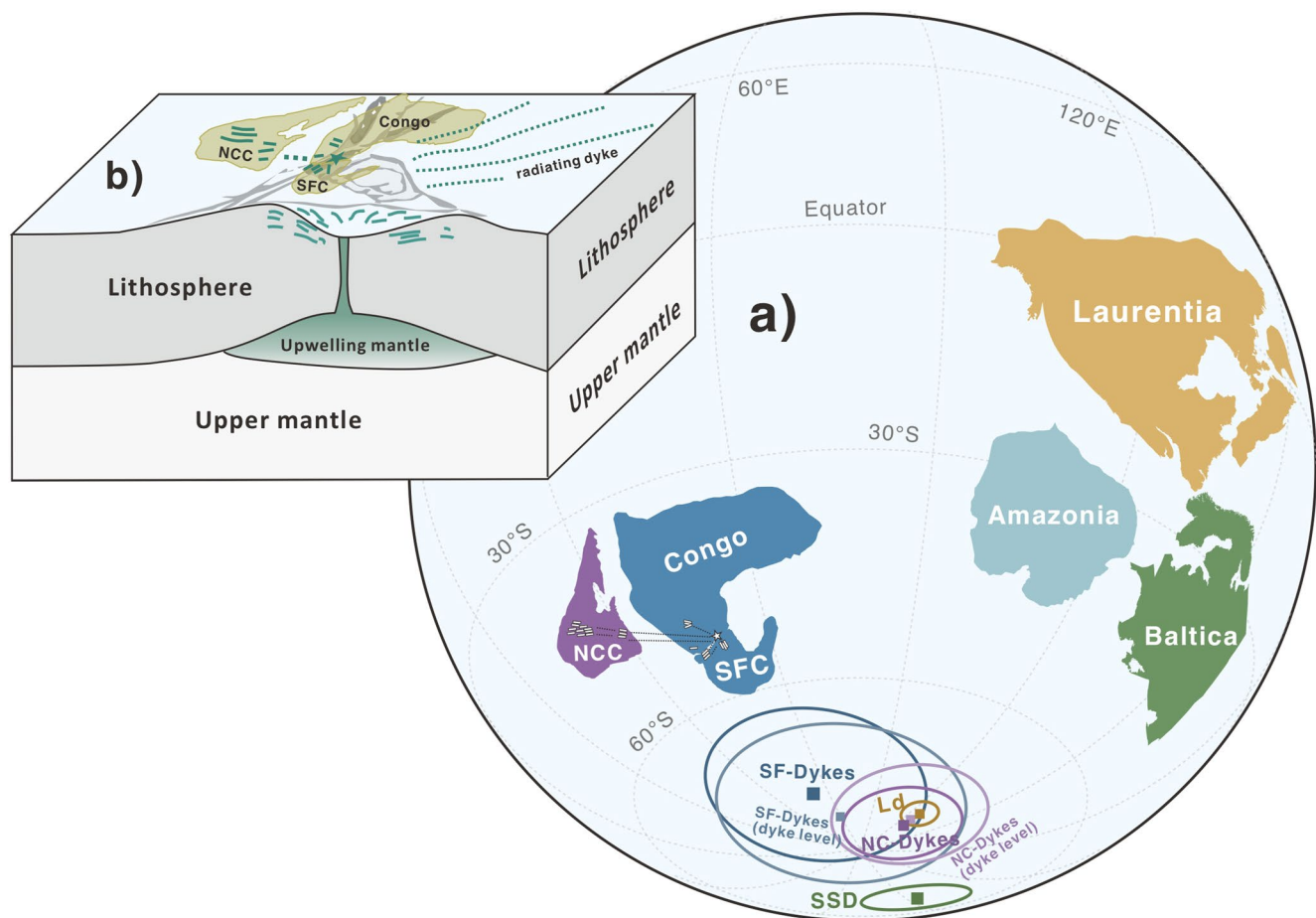


**Figure 11.** (a) Paleogeographic reconstruction for the North China craton (NCC), São Francisco Craton (SFC) and other major building cratons (Congo, Amazonia, Laurentia and Baltica) of the Rodinia during 925 Ma. Cratons and their poles (SF-Dykes, NC-Dykes, Ld and SSD, see details in Table 3) are matched in color. In the reconstruction, the following Euler poles are used: 45.31°N, 162.32°E, 174.19° for Laurentia; 7.27°N, 202.18°E, -139.83° for Amazonia; 38.04°N, 185.30°E, 139.70° for Baltica; 5.54°N, 194.30°E, -100.37° for SFC, 39.28°N, 331.61°E, -116.12° for NCC and 9.13°N, 232.05°E, -88.88 for Congo Craton. The positions of Amazonia and Baltica relative to Laurentia (in its present position) are the same proposed by Merdith et al. (2017) (Euler pole: 11.9°N, -47.0°E, -110.6°) and Evans (2009) (Euler pole at: 81.5°N, 250.0°E, -50.0°), respectively. The position of the Congo Craton relative to SFC is the same proposed by McElhinny et al. (2003) (Euler pole: 40.2°N, 26.5°E, -178.9°) for the pre-Atlantic Ocean configuration. (b) Cartoon showing a radiating mafic dyke system driven by upwelling asthenosphere speculated to comprise coeval mafic dykes in the NCC and SFC, modified from Su et al. (2021). The star and dashed lines represent the speculated mantle plume and flow directions, modified from Peng, Bleeker, et al. (2011).

The characteristic remanence of the 925 Ma dykes in the two cratons was interpreted to be primary. The results imply that the NCC and SFC were located southwest of Laurentia in the moderate to high paleolatitudes of the Southern Hemisphere during 925 Ma, suggesting a paleogeographic connection between the two cratons in Rodinia. The geographic proximity between the NCC and SFC is consistent with geological and geophysical evidence including dyke geometry, magma emplacement mode, provenance characteristics, and correlatable basin history between the cratons. The new configuration between the NCC and SFC is also more contingent with their involvements in subsequent tectonic models. Additional paleomagnetic and geologic data are needed to verify the southern paleolatitudes of both cratons during the Neoproterozoic, and test and refine this paleogeographic reconstruction of Rodinia at 925 Ma.

### Data Availability Statement

The detailed paleomagnetic data of the NCC and São Francisco Craton used for paleogeographic reconstruction in this study are in Supporting Information S1 and also available at MagIC via <https://earthref.org/MagIC/19478/ac2a2508-3d42-4539-be7c-16fa3caf9fc3>. Other paleomagnetic data in this study can be downloaded from the PALEOMAGIA database via <https://paleomagia.it.helsinki.fi/> (Veikkolainen et al., 2017).

### Acknowledgments

We wish to acknowledge the expertise, helpful advice, and continuing discussions generously provided by Drs. Mingguo Zhai, Shihong Zhang, Baochun Huang, Ricardo Trindade, Elson Oliveira, Wilson Teixeira, Qingsong Liu and Mr. Wei Cao. We thank Drs. Farid Chemale Jr., Elson Paiva de Oliveira and Wei Yuan for their help with sample collection and measurement, and Dr. Lingmin Zhang for SEM analyses. We also extend our thanks to the journal reviewers for their constructive comments and suggestions, and Editor Dr. Mark Dekkers and Associate Editor Dr. Adrian Muxworthy for their useful comments and efficient editorial handling. All these comments significantly improved the manuscript. This study was financially supported by the National Natural Science Foundation of China (Nos. 41874076, 41890833, 92158207), and the National Key Research & Development Project (Grant No. 2016YFC0601005).

### References

- Alkmim, F. F., & Marshak, S. (1998). Transamazonian orogeny in the Southern São Francisco craton region, Minas Gerais, Brazil: Evidence for Paleoproterozoic collision and collapse in the Quadrilátero Ferrífero. *Precambrian Research*, *90*(1–2), 29–58. [https://doi.org/10.1016/S0301-9268\(98\)00032-1](https://doi.org/10.1016/S0301-9268(98)00032-1)
- Barbosa, J. F. S., Peucat, J.-J., Martine, H., da Silva, F. A., Moraes, A. M., Corrêas-Gomes, L. C., et al. (2008). Petrogenesis of the late-orogenic Bravo granite and surrounding high-grade country rocks in the Palaeoproterozoic orogen of Itabuna-Salvador-Curacá block, Bahia, Brazil. *Precambrian Research*, *167*(1–2), 35–52. <https://doi.org/10.1016/j.precamres.2008.06.002>
- Bellieni, G., Petrini, R., Piccirillo, E. M., Brito, C. M., Figueiredo, A. M. G., Marques, L. S., et al. (1998). Petrogenesis and tectonic significance of the Late Proterozoic unmetamorphosed mafic dyke swarms from the Salvador area (NE Brazil). *Neues Jahrbuch für Mineralogie—Abhandlungen*, *173*(3), 327–350. <https://doi.org/10.1127/njma/173/1998/327>
- Bryan, S. E., & Ernst, R. E. (2008). Revised definition of large igneous provinces (LIPs). *Earth-Science Reviews*, *86*(1–4), 175–202. <https://doi.org/10.1016/j.earscirev.2007.08.008>
- Burrett, C., Long, J., & Stait, B. (1990). Early-Middle Palaeozoic biogeography of Asian terranes derived from Gondwana. *Geological Society, London, Memoirs*, *12*(1), 163–174. <https://doi.org/10.1144/GSL.MEM.1990.012.01.14>
- Cawood, P. A., Strachan, R. A., Pisarevsky, S. A., Gladkochub, D. P., & Murphy, J. B. (2016). Linking collisional and accretionary orogens during Rodinia assembly and breakup: Implications for models of supercontinent cycles. *Earth and Planetary Science Letters*, *449*, 118–126. <https://doi.org/10.1016/j.epsl.2016.05.049>
- Caxito, F. A., Hagemann, S., Dias, T. G., Barrote, V., Dantas, E. L., de Oliveira Chaves, A., et al. (2020). A magmatic barcode for the São Francisco Craton: Contextual in-situ SHRIMP UPb baddeleyite and zircon dating of the Lavras, Pará de Minas and Formiga dyke swarms and implications for Columbia and Rodinia reconstructions. *Lithos*, *374*, 105708. <https://doi.org/10.1016/j.lithos.2020.105708>
- Cederberg, J., Söderlund, U., Oliveira, E. P., Ernst, R. E., & Pisarevsky, S. A. (2016). U-Pb baddeleyite dating of the Proterozoic Pará de Minas dyke swarm in the São Francisco craton (Brazil)—implications for tectonic correlation with the Siberian, Congo and North China cratons. *GFF*, *138*(1), 219–240. <https://doi.org/10.1080/11035897.2015.1093543>
- Chaves, A. O., Ernst, R. E., Söderlund, U., Wang, X., & Naeraa, T. (2019). The 920–900 Ma Bahia-Gangila LIP of the São Francisco and Congo cratons and link with Dashigou-Chulan LIP of North China craton: New insights from U-Pb geochronology and geochemistry. *Precambrian Research*, *329*, 124–137. <https://doi.org/10.1016/j.precamres.2018.08.023>
- Chen, L., Huang, B., Yi, Z., Zhao, J., & Yan, Y. (2013). Paleomagnetism of ca. 1.35 Ga sills in northern North China Craton and implications for paleogeographic reconstruction of the Mesoproterozoic supercontinent. *Precambrian Research*, *228*, 36–47. <https://doi.org/10.1016/j.precamres.2013.01.011>
- Condie, K. C. (2002). Breakup of a Paleoproterozoic supercontinent. *Gondwana Research*, *5*(1), 41–43. [https://doi.org/10.1016/S1342-937X\(05\)70886-8](https://doi.org/10.1016/S1342-937X(05)70886-8)
- Cordani, U. G., Teixeira, W., D'Agrella-Filho, M. S., & Trindade, R. I. (2009). The position of the Amazonian Craton in supercontinents. *Gondwana Research*, *15*(3–4), 396–407. <https://doi.org/10.1016/j.gr.2008.12.005>
- Correa-Gomes, L. C., & Oliveira, E. P. (2000). Radiating 1.0 Ga mafic dyke swarms of eastern Brazil and Western Africa: Evidence of post-assembly extension in the Rodinia supercontinent? *Gondwana Research*, *3*(3), 325–332. [https://doi.org/10.1016/S1342-937X\(05\)70291-4](https://doi.org/10.1016/S1342-937X(05)70291-4)
- Cox, A. (1970). Latitude dependence of the angular dispersion of the geomagnetic field. *Geophysical Journal International*, *20*(3), 253–269. <https://doi.org/10.1111/j.1365-246X.1970.tb06069.x>
- D'Agrella-Filho, M. S., Pacca, I. G., Renne, P. R., Onstott, T. C., & Teixeira, W. (1990). Paleomagnetism of middle proterozoic (1.01 to 1.08 Ga) mafic dykes in southeastern Bahia State—São Francisco craton, Brazil. *Earth and Planetary Science Letters*, *101*(2–4), 332–348. [https://doi.org/10.1016/0012-821X\(90\)90164-5](https://doi.org/10.1016/0012-821X(90)90164-5)
- D'Agrella-Filho, M. S., Pacca, I. I., Trindade, R. I., Teixeira, W., Raposo, M. I. B., & Onstott, T. C. (2004). Paleomagnetism and <sup>40</sup>Ar/<sup>39</sup>Ar ages of mafic dikes from Salvador (Brazil): New constraints on the São Francisco craton APW path between 1080 and 1010 Ma. *Precambrian Research*, *132*(1–2), 55–77. <https://doi.org/10.1016/j.precamres.2004.02.003>
- D'Agrella-Filho, M. S., Teixeira, W., da Trindade, R. I., Patroni, O. A., & Prieto, R. F. (2020). Paleomagnetism of 1.79 Ga Pará de Minas mafic dykes: Testing a São Francisco/Congo-North China-Rio de la Plata connection in Columbia. *Precambrian Research*, *338*, 105584. <https://doi.org/10.1016/j.precamres.2019.105584>
- Day, R., Fuller, M., & Schmidt, V. A. (1977). Hysteresis properties of titanomagnetites: Grain-size and compositional dependence. *Physics of the Earth and Planetary Interiors*, *13*(4), 260–267. [https://doi.org/10.1016/0031-9201\(77\)90108-X](https://doi.org/10.1016/0031-9201(77)90108-X)
- Deenen, M. H. L., Langereis, C. G., van Hinsbergen, D. J. J., & Biggin, A. J. (2011). Geomagnetic secular variation and the statistics of palaeomagnetic directions. *Geophysical Journal International*, *186*(2), 509–520. <https://doi.org/10.1111/j.1365-405246X.2011.05050.x>
- Doucet, L. S., Li, Z. X., Ernst, R. E., Kirscher, U., El Dien, H. G., & Mitchell, R. N. (2020). Coupled supercontinent–mantle plume events evidenced by oceanic plume record. *Geology*, *48*(2), 159–163. <https://doi.org/10.1130/G46754.1>
- Elming, S. Å., Pisarevsky, S. A., Layer, P., & Bylund, G. (2014). A palaeomagnetic and <sup>40</sup>Ar/<sup>39</sup>Ar study of mafic dykes in southern Sweden: A new early neoproterozoic key-pole for the Baltic Shield and implications for Sveconorwegian and Grenville loops. *Precambrian Research*, *244*, 192–206. <https://doi.org/10.1016/j.precamres.2013.12.007>
- Elston, D. P., Enkin, R. J., Baker, J., & Kisilevsky, D. K. (2002). Tightening the belt: Paleomagnetic-stratigraphic constraints on deposition, correlation, and deformation of the middle proterozoic (ca. 1.4 Ga) belt–Purcell Supergroup, United States and Canada. *The Geological Society of America Bulletin*, *114*(5), 619–638. [https://doi.org/10.1130/0016-7606\(2002\)114<0619:TTBPSC>2.0.CO;2](https://doi.org/10.1130/0016-7606(2002)114<0619:TTBPSC>2.0.CO;2)
- Ernst, R. E., & Buchan, K. L. (1997). *Giant radiating dyke swarms: Their use in identifying pre-Mesozoic large igneous provinces and mantle plumes* (Vol. 100, pp. 297–334). Geophysical Monograph–American Geophysical Union. <https://doi.org/10.1029/GM100p0297>
- Ernst, R. E., Wingate, M. T. D., Buchan, K. L., & Li, Z. X. (2008). Global record of 1600–700 Ma large igneous provinces (LIPs): Implications for the reconstruction of the proposed Nuna (Columbia) and Rodinia supercontinents. *Precambrian Research*, *160*(1–2), 159–178. <https://doi.org/10.1016/j.precamres.2007.04.019>
- Evans, D. A. (2009). The palaeomagnetically viable, long-lived and all-inclusive Rodinia supercontinent reconstruction. *Geological Society, London, Special Publications*, *327*(1), 371–404. <https://doi.org/10.1144/SP327.16>
- Evans, D. A. D., Trindade, R. I. F., Catelani, E. L., D'Agrella-Filho, M. S., Heaman, L. M., Oliveira, E. P., et al. (2016). Return to Rodinia? Moderate to high palaeolatitude of the São Francisco/Congo craton at 920 Ma. *Geological Society, London, Special Publications*, *424*(1), 167–190. <https://doi.org/10.1144/SP424.1>
- Fisher, R. A. (1953). Dispersion on a sphere. *Proceedings of the Royal Society of London. Series A. Mathematical and Physical Sciences*, *217*(1130), 295–305. <https://doi.org/10.1098/rspa.1953.0064>

- Flinn, D. (1965). On the symmetry principle and the deformation ellipsoid. *Geological Magazine*, 102(1), 36–45. <https://doi.org/10.1017/S0016756800053851>
- Fu, X., Zhang, S., Li, H., Ding, J., Li, H., Yang, T., et al. (2015). New paleomagnetic results from the Huaibei Group and Neoproterozoic mafic sills in the North China Craton and their paleogeographic implications. *Precambrian Research*, 269, 90–106. <https://doi.org/10.1016/j.precamres.2015.08.013>
- Halls, H. C., Li, J., Davis, D., Hou, G., Zhang, B., & Qian, X. (2000). A precisely dated Proterozoic palaeomagnetic pole from the North China craton, and its relevance to palaeocontinental reconstruction. *Geophysical Journal International*, 143(1), 185–203. <https://doi.org/10.1016/j.precamres.2013.01.011>
- Hrouda, F. (1982). Magnetic anisotropy of rocks and its application in geology and geophysics. *Geophysical Surveys*, 5(1), 37–82. <https://doi.org/10.1007/bf01450244>
- Huang, B., Yan, Y., Piper, J. D., Zhang, D., Yi, Z., Yu, S., & Zhou, T. (2018). Paleomagnetic constraints on the paleogeography of the East Asian blocks during late Paleozoic and Early Mesozoic times. *Earth-Science Reviews*, 186, 8–36. <https://doi.org/10.1016/j.earscirev.2018.02.004>
- Huang, B., Yang, Z., Otofujii, Y. I., & Zhu, R. (1999). Early Paleozoic paleomagnetic poles from the Western part of the North China Block and their implications. *Tectonophysics*, 308(3), 377–402. [https://doi.org/10.1016/S0040-1951\(99\)00098-0](https://doi.org/10.1016/S0040-1951(99)00098-0)
- Huang, B., Zhu, R., Otofujii, Y. A., & Yang, Z. (2000). The Early Paleozoic paleogeography of the North China block and the other major blocks of China. *Chinese Science Bulletin*, 45(12), 1057–1065. <https://doi.org/10.1007/BF02887174>
- Kirschvink, J. (1980). The least-squares line and plane and the analysis of palaeomagnetic data. *Geophysical Journal International*, 62(3), 699–718. <https://doi.org/10.1111/j.1365-246X.1980.tb02601.x>
- Knight, M. D., & Walker, G. P. (1988). Magma flow directions in dikes of the Koolau Complex, Oahu, determined from magnetic fabric studies. *Journal of Geophysical Research*, 93(B5), 4301–4319. <https://doi.org/10.1029/JB093iB05p04301>
- Koopmans, L., McCarthy, W., & Magee, C. (2022). Dyke Architecture, mineral layering, and magmatic convection; New Perspectives from the younger giant dyke complex, S Greenland. *Geochemistry, Geophysics, Geosystems*, 23(3), e2021GC010260. <https://doi.org/10.1029/2021GC010260>
- Li, Z. X., Bogdanova, S., Collins, A. S., Davidson, A., De Waele, B., Ernst, R. E., et al. (2008). Assembly, configuration, and break-up history of Rodinia: A synthesis. *Precambrian Research*, 160(1–2), 179–210. <https://doi.org/10.1016/j.precamres.2007.04.021>
- Li, Z. X., Zhang, L., & Powell, C. M. (1996). Positions of the East Asian cratons in the neoproterozoic supercontinent Rodinia. *Australian Journal of Earth Sciences*, 43(6), 593–604. <https://doi.org/10.1080/08120099608728281>
- Li, Z. X., & Zhong, S. (2009). Supercontinent–superplume coupling, true polar wander and plume mobility: Plate dominance in whole-mantle tectonics. *Physics of the Earth and Planetary Interiors*, 176(3–4), 143–156. <https://doi.org/10.1016/j.pepi.2009.05.004>
- Lin, J. (1984). *The apparent polar wander paths for the north and south China blocks (Doctoral dissertation)*. University California.
- Loureiro, H. S. C., Lima, E. S., Macedo, E. P., Bahiense, J. B. A., Neves, J. P., Guimarães, J. T., et al. (2008). *Projeto Barra-Oliveira dos Brejinhos*. CPRM. Retrieved from <https://rigeo.cprm.gov.br/handle/doc/21793>
- McElhinny, M. W., Powell, C. M., & Pisarevsky, S. A. (2003). Paleozoic terranes of eastern Australia and the drift history of Gondwana. *Tectonophysics*, 362(1–4), 41–65. [https://doi.org/10.1016/S0040-1951\(02\)00630-3](https://doi.org/10.1016/S0040-1951(02)00630-3)
- McFadden, P. L., & McElhinny, M. W. (1990). Classification of the reversal test in palaeomagnetism. *Geophysical Journal International*, 103(3), 725–729. <https://doi.org/10.1111/j.1365-246X.1990.tb05683.x>
- McMenamin, M. A., & McMenamin, D. L. S. (1990). *The Emergence of Animals the Cambrian Breakthrough*. Columbia University Press. <https://doi.org/10.7312/mcme93416>
- Merdith, A. S., Collins, A. S., Williams, S. E., Pisarevsky, S., Foden, J. D., Archibald, D. B., et al. (2017). A full-plate global reconstruction of the Neoproterozoic. *Gondwana Research*, 50, 84–134. <https://doi.org/10.1016/j.gr.2017.04.001>
- Merdith, A. S., Williams, S. E., Brune, S., Collins, A. S., & Müller, R. D. (2019). Rift and plate boundary evolution across two supercontinent cycles. *Global and Planetary Change*, 173, 1–14. <https://doi.org/10.1016/j.gloplacha.2018.11.006>
- Moore, E. M. (1991). Southwest US–East Antarctic (SWEAT) connection: A hypothesis. *Geology*, 19(5), 425–428. [https://doi.org/10.1130/0091-7613\(1991\)019<0425:SUSEAS>2.3.CO;2](https://doi.org/10.1130/0091-7613(1991)019<0425:SUSEAS>2.3.CO;2)
- Moreira, H. F., Danderfer, A., Costa, A. F., Bersan, S. M., Lana, C. C., & Queiroga, G. N. (2020). Record of Early Tonian mafic magmatism in the central Espinhaço (Brazil): New insights for break-up of the Neoproterozoic landmass ancestor of São Francisco–Congo paleocontinent. *Geoscience Frontiers*, 11(6), 2323–2337. <https://doi.org/10.1016/j.gsf.2020.02.007>
- Nance, R. D., & Murphy, J. B. (2013). Origins of the supercontinent cycle. *Geoscience Frontiers*, 4(4), 439–448. <https://doi.org/10.1016/j.gsf.2012.12.007>
- Nance, R. D., Worsley, T. R., & Moody, J. B. (1988). The supercontinent cycle. *Scientific American*, 259(1), 72–79. <https://doi.org/10.1038/scientificamerican0788-72>
- Padilha, A. L., Vitorello, I., de Padua, M. B., & Fuck, R. A. (2019). Magnetotelluric images of Paleoproterozoic accretion and Mesoproterozoic to Neoproterozoic reworking processes in the northern São Francisco Craton, central-eastern Brazil. *Precambrian Research*, 333, 105416. <https://doi.org/10.1016/j.precamres.2019.105416>
- Peng, P. (2010). Reconstruction and interpretation of giant mafic dyke swarms: A case study of 1.78 Ga magmatism in the North China craton. *Geological Society, London, Special Publications*, 338(1), 163–178. <https://doi.org/10.1144/SP338.8>
- Peng, P. (2015a). Late Paleoproterozoic–neoproterozoic (1800–541 Ma) mafic dyke swarms and rifts in North China. In *Precambrian geology of China* (pp. 171–204). Springer. [https://doi.org/10.1007/978-3-662-47885-1\\_4](https://doi.org/10.1007/978-3-662-47885-1_4)
- Peng, P. (2015b). Precambrian mafic dyke swarms in the North China Craton and their geological implications. *Science China Earth Sciences*, 58(5), 649–675. <https://doi.org/10.1007/s11430-014-5026-x>
- Peng, P., Bleeker, W., Ernst, R. E., Söderlund, U., & McNicoll, V. (2011). U–Pb baddeleyite ages, distribution and geochemistry of 925 Ma mafic dykes and 900 Ma sills in the North China craton: Evidence for a neoproterozoic mantle plume. *Lithos*, 127(1–2), 210–221. <https://doi.org/10.1016/j.lithos.2011.08.018>
- Peng, P., Zhai, M. G., Li, Q., Wu, F., Hou, Q., Li, Z., et al. (2011b). Neoproterozoic (~900 Ma) Sariwon sills in North Korea: Geochronology, geochemistry and implications for the evolution of the South-eastern margin of the North China Craton. *Gondwana Research*, 20(1), 243–254. <https://doi.org/10.1016/j.gr.2010.12.011>
- Raposo, M. I. B., & Berquó, T. S. (2008). Tectonic fabric revealed by AARM of the proterozoic mafic dike swarm in the Salvador city (Bahia State): São Francisco Craton, NE Brazil. *Physics of the Earth and Planetary Interiors*, 167(3–4), 179–194. <https://doi.org/10.1016/j.pepi.2008.03.012>
- Su, X., Peng, P., Foley, S., Teixeira, W., & Zhai, M. G. (2021). Initiation of continental breakup documented in evolution of the magma plumbing system of the ca. 925 Ma Dashigou large igneous province, North China. *Lithos*, 384, 105984. <https://doi.org/10.1016/j.lithos.2021.105984>

- Sun, F., Peng, P., Zhou, X., Magalhaes, A. J. C., Guadagnin, F., Zhou, X., et al. (2020). Provenance analysis of the late Mesoproterozoic to neoproterozoic Xuhuai basin in the southeast North China Craton: Implications for paleogeographic reconstruction. *Precambrian Research*, 337, 105554. <https://doi.org/10.1016/j.precamres.2019.105554>
- Tang, Y. J., Zhang, H. F., Deloule, E., Su, B. X., Ying, J. F., Xiao, Y., & Hu, Y. (2012). Slab-derived lithium isotopic signatures in mantle xenoliths from northeastern North China Craton. *Lithos*, 149, 79–90. <https://doi.org/10.1016/j.lithos.2011.12.001>
- Teixeira, W., Oliveira, E. P., & Marques, L. S. (2017). Nature and evolution of the Archean crust of the São Francisco Craton. In *São Francisco craton, Eastern Brazil* (pp. 29–56). Springer. [https://doi.org/10.1007/978-3-319-01715-0\\_3](https://doi.org/10.1007/978-3-319-01715-0_3)
- Trindade, R. I., D'Agrella-Filho, M. S., Antonio, P. Y., & Teixeira, W. (2021). The Precambrian drift history and paleogeography of Congo-São Francisco craton. In *Ancient supercontinents and the paleogeography of Earth* (pp. 445–464). Elsevier. <https://doi.org/10.1016/B978-0-12-818533-9.00016-3>
- Van der Voo, R. (1990). The reliability of paleomagnetic data. *Tectonophysics*, 184(1), 1–9. [https://doi.org/10.1016/0040-1951\(90\)90116-P](https://doi.org/10.1016/0040-1951(90)90116-P)
- Veikkolainen, T. H., Biggin, A. J., Pesonen, L. J., Evans, D. A., & Jarboe, N. A. (2017). Advancing Precambrian palaeomagnetism with the PALEOMAGIA and PINT (QPI) databases [Dataset]. Scientific Data, 4(1), 1–10. <https://doi.org/10.1038/sdata.2017.68>
- Wang, L. J., Guo, J. H., Yin, C., & Peng, P. (2017). Petrogenesis of ca. 1.95 Ga meta-leucogranites from the Jining complex in the Khondalite belt, North China Craton: Water-fluxed melting of metasedimentary rocks. *Precambrian Research*, 303, 355–371. <https://doi.org/10.1016/j.precamres.2017.04.036>
- Xu, H., Yang, Z., Peng, P., Meert, J. G., & Zhu, R. (2014). Paleo-position of the North China craton within the supercontinent Columbia: Constraints from new paleomagnetic results. *Precambrian Research*, 255, 276–293. <https://doi.org/10.1016/j.precamres.2014.10.004>
- Zhai, M., Hu, B., Zhao, T., Peng, P., & Meng, Q. (2015). Late Paleoproterozoic–neoproterozoic multi-rifting events in the North China Craton and their geological significance: A study advance and review. *Tectonophysics*, 662, 153–166. <https://doi.org/10.1016/j.tecto.2015.01.019>
- Zhang, J., & Piper, J. D. (1994). Magnetic fabric and post-orogenic uplift and cooling magnetisations in a Precambrian granulite terrain: The Datong-Huai'an region of the North China Shield. *Tectonophysics*, 234(3), 227–246. [https://doi.org/10.1016/0040-1951\(94\)90213-5](https://doi.org/10.1016/0040-1951(94)90213-5)
- Zhang, S., Chang, L., Zhao, H., Ding, J., Xian, H., Li, H., et al. (2021). The Precambrian drift history and paleogeography of the Chinese cratons. In *Ancient supercontinents and the paleogeography of Earth* (pp. 333–376). Elsevier. <https://doi.org/10.1016/B978-0-12-818533-9.00005-9>
- Zhang, S., Li, Z. X., Evans, D. A., Wu, H., Li, H., & Dong, J. (2012). Pre-Rodinia supercontinent Nuna shaping up: A global synthesis with new paleomagnetic results from North China. *Earth and Planetary Science Letters*, 353, 145–155. <https://doi.org/10.1016/j.epsl.2012.07.034>
- Zhang, S., Li, Z. X., & Wu, H. (2006). New Precambrian palaeomagnetic constraints on the position of the North China block in Rodinia. *Precambrian Research*, 144(3–4), 213–238. <https://doi.org/10.1016/j.precamres.2005.11.007>
- Zhao, G., & Cawood, P. A. (2012). Precambrian geology of China. *Precambrian Research*, 222, 13–54. <https://doi.org/10.1016/j.precamres.2012.09.017>
- Zhao, G., Wang, Y., Huang, B., Dong, Y., Li, S., Zhang, G., & Yu, S. (2018). Geological reconstructions of the East Asian blocks: From the breakup of Rodinia to the assembly of Pangea. *Earth-Science Reviews*, 186, 262–286. <https://doi.org/10.1016/j.earscirev.2018.10.003>
- Zhao, H., Zhang, S., Ding, J., Chang, L., Ren, Q., Li, H., et al. (2020). New geochronologic and paleomagnetic results from early Neoproterozoic mafic sills and late Mesoproterozoic to early Neoproterozoic successions in the eastern North China Craton, and implications for the reconstruction of Rodinia. *GSA Bulletin*, 132(3–4), 739–766. <https://doi.org/10.1130/B35198.1>
- Zhao, X., Coe, R. S., Zhou, Y., Hu, S., Wu, H., Kuang, G., et al. (1994). Tertiary paleomagnetism of North and South China and a reappraisal of late Mesozoic paleomagnetic data from Eurasia: Implications for the cenozoic tectonic history of Asia. *Tectonophysics*, 235(1–2), 181–203. [https://doi.org/10.1016/0040-1951\(94\)90023-X](https://doi.org/10.1016/0040-1951(94)90023-X)
- Zijderveld, J. D. A. (1967). AC demagnetization of rocks. *Methods in Palaeomagnetism*, 254–286.